JOURNAL OF GEOPHYSICAL RESEARCH, VOL. 99, NO. C6, PAGES 12,319–12,341, JUNE 15, 1994

The production of North Atlantic Deep Water: Sources, rates, and pathways

Robert R. Dickson and Juan Brown

Fisheries Laboratory, Directorate of Fisheries Research, Ministry of Agriculture, Fisheries, and Food, Lowestoft, Suffolk, England

Abstract. Updating an earlier account by Dickson et al., (1990), this paper reviews the initial development phase of North Atlantic Deep Water (NADW) production from the points where the dense inflows from Nordic seas cross the Greenland-Scotland Ridge to the point off south Greenland where the buildup of new production appears almost complete. In particular, three long-term current meter arrays totaling 91 instruments and set at ~160 km intervals south from the Denmark Strait sill are used to validate earlier short-term arrays by others and, in combination with these earlier arrays, to describe the downstream evolution of mean speed, depth and entrainment, the variability of the overflow current in space and time, and the likely contribution of the other three main constituents of NADW production at densities greater than $\sigma\theta = 27.8$. From the points of overflow (5.6 Sv) the transport within this range increases by entrainment and confluence with other contributory streams to around 13.3 Sv at Cape Farewell. While recirculating elements prevent us from determining the net southgoing transport, a NADW transport of this order appears consistent with recent estimates of net abyssal flow passing south through the North and South Atlantic.

1. Introduction

The global thermohaline circulation, driven by fluxes of heat and fresh water at the ocean surface, is an important mechanism for the global redistribution of heat and salt and is known to be intimately involved in the major changes in earth climate. For example, a partial shutdown of this world-wide overturning cell appears to have accompanied each abrupt shift of the ocean-atmosphere system toward glaciation [*Broecker and Denton*, 1989].

In turn, the thermohaline circulation is driven by inputs of dense water from two high-latitude sources, (1) the input of North Atlantic Deep Water (NADW) in the northern North Atlantic and (2) the outflow of Antarctic Bottom Water (AABW) formed at various sites on the continental shelf of Antarctica during austral winter [*Warren*, 1981] but principally formed (~80%) in the Weddell Sea [*Foldvik and Gammelsrod*, 1988].

On the millennial timescales which describe the glacial/postglacial signal the δC_{13} record in benthic forams from Southern Ocean sediments is interpreted as showing radical and rapid change in the production and flux of NADW in the abyssal circulation [*Charles and Fairbanks*, 1992]. Our knowledge of its present-day production, however, remains poor.

This paper is intended to update an earlier report by *Dickson et al.* [1990] by describing the renewal, variability (where known), and pathways of the four main constituents of NADW through the northern North Atlantic. The primary aim, however, is to provide a more detailed description than currently exists for the Denmark Strait Overflow component using a large body of new and direct observational evidence.

Paper number 94JC00530.
0148-0227/94/94JC-00530$05.00

Past Schemes for NADW Production and Transport

As *Broecker and Peng* [1982, p. 317] point out, a more realistic quantitative representation of the ventilation of the deep sea "remains one of the major unsolved problems in oceanography." The most famous papers of a series describing schemes for deep ventilation and exchange in the northern gyre are those by *Worthington* [1970, 1976] and *McCartney and Talley* [1984]. Although these schemes (Figures 1a–1c) derive more or less the same value for the transport of the Deep Western Boundary Current (DWBC) where it passes south through 50°N (10 Sv in both of *Worthington*'s [1970, 1976] schemes and 11.1 Sv in one case described by *McCartney and Talley* [1984]; 1 Sv = 10^6 m^3 s^{-1}), these numbers are in fact based on completely different sets of assumptions, suggesting that the available range of conjecture is too wide to be useful.

For example, although *Worthington*'s [1970, 1976] schemes both imply a 10 Sv DWBC passing through 50°N, they differ so much in detail that the one balances twice as much heat flux at high latitudes as the other (60% and 27%, respectively, of Bunker's value of 87 × 10^{12} cal s^{-1} [see *McCartney and Talley*, 1984, p. 927]). Moreover, although both of *Worthington*'s [1970, 1976] schemes assume that all of the deep water going south through 50°N originates north of the Greenland-Scotland Ridge, *McCartney and Talley* [1984] discount the importance of these overflows and instead suggest that three-quarters of the deep flow through 50°N is formed in the Labrador Sea (8.5 Sv from deepwater renewal in the Labrador Sea; 2.5 Sv from overflows crossing the Greenland-Scotland Ridge).

The confusion is made worse by some fundamental oversights and errors. As *Aagaard and Carmack* [1989, p. 14, 494] point out, *Worthington*'s [1970] contention "that the principal water mass transformation in the GIN (i.e., Greenland-Iceland-Norwegian) Sea is the cooling of waters drawn

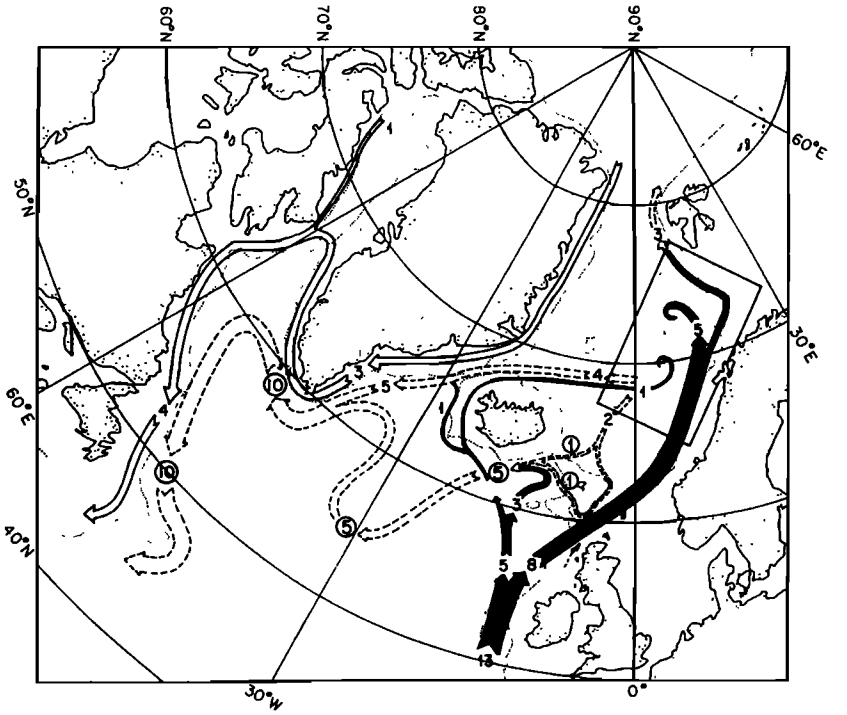

Figure 1a. *Worthington*'s [1970] scheme for watermass conversion flow paths in the northern North Atlantic. Warm (>4°C) currents are denoted by solid black arrows; the curled ends denote sinking. Cold currents are denoted by open arrows, with light and dense overflows shown by solid and dashed lines, respectively. Circled numbers are transport estimates in Sverdrups, where 1 Sv = 10^6 m^3 s^{-1}.

in from the North Atlantic, and that this transformation is the necessary precursor to the renewal of the North Atlantic Deep Water . . . ignores the fact that the dense outflows to the North Atlantic are significantly fresher than the warm inflows. Thereby it also ignores the implications of that freshening on water mass transformation and convection within the GIN Sea." *Aagaard and Carmack* [1989] also criticize the fact that *Worthington*'s [1970] estimates of

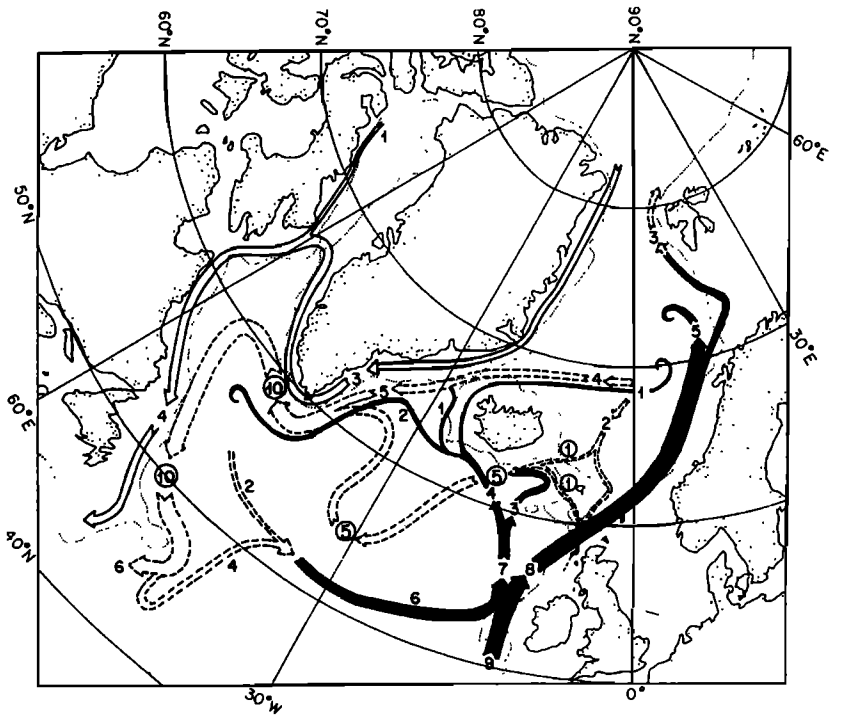

Figure 1b. The recasting of *Worthington*'s [1970] scheme by *McCartney and Talley* [1984], based on *Worthington*'s [1976] box model. Notation is the same as Figure 1a.

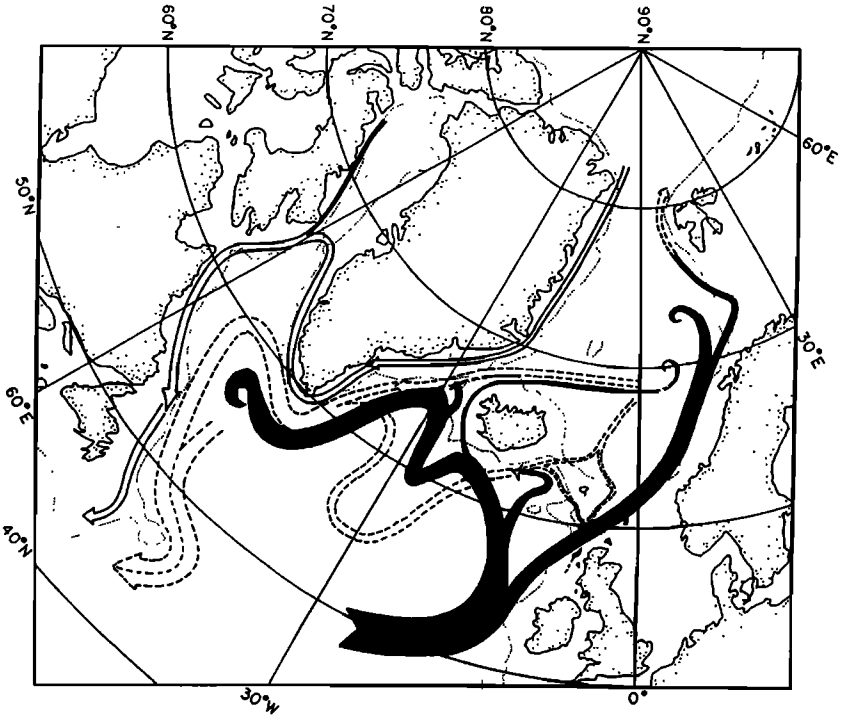

Figure 1c. The further modification of *Worthington*'s [1970] scheme proposed by *McCartney and Talley* [1984]. Notation is the same as Figure 1a.

transport west of 35°W all use the core of the Labrador Sea Water as a level of no motion.

Despite such points of criticism, these works by Worthington and McCartney and Talley are milestones in our attempts to understand and portray the processes of ventilation and exchange in the northern gyre. However, it is plain that the business of refining these schemes could not usefully advance without further measurements to guide the process, simply because there are any number of scenarios for balancing our imprecise notions of high-latitude heat flux by interbasin transports at prescribed temperatures.

The Sources of NADW

Figure 2 (from *Swift* [1984]) indicates the locus of NADW on the potential temperature-salinity diagram for North Atlantic Deep Waters colder than 4°C and was adapted by Swift from *Worthington and Wright*'s [1970] volumetric census. The hatched potential temperature-salinity classes enclose some 51% of total deep-water volume and show the influence of four main contributory components. Of these, Labrador Sea Water (LSW) is the warmest and shallowest and fans out in four broad tongues from its source area in the Labrador Sea. It is readily traceable by a vertical minimum of potential vorticity which is very nearly an isopycnal but lies too deep to cross the Greenland-Scotland Ridge to enter the Greenland-Iceland-Norwegian Sea. These and other characteristics of LSW are described by *Talley and McCartney* [1982].

Where LSW spreads into the Irminger and South Icelandic Basins, it overlies and exchanges with the other two principal source water masses, which overflow the Greenland-Scotland Ridge on either side of Iceland from intermediate depths in the Greenland Sea. The sill depths alone, 600 m in the Denmark Strait, ~450 m on the Iceland-Faroe Ridge, and ~850 m in the Faroe Bank Channel, mean that these overflows are not the product of deep convection but of intermediate water formation north of the Greenland-Scotland Ridge. As *Swift* [1984, Figure 6] shows, the σ_2 = 37.04 isopycnal surface lies at >3250 m depth in the Newfoundland Basin but lies at <250 m north of the Denmark Strait and in the southern Norwegian Sea, and in the

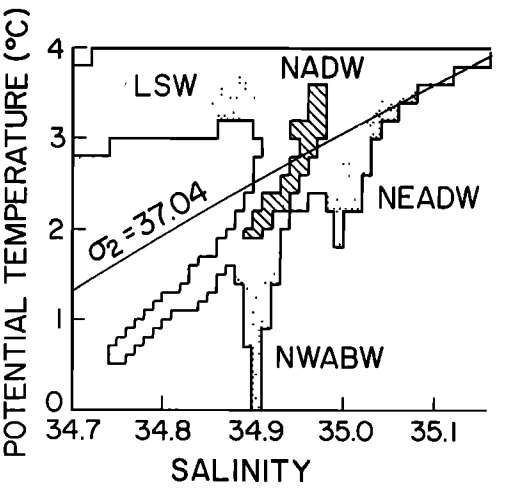

Figure 2. Potential temperature-salinity diagram for North Atlantic Deep Waters colder than 4°C, adapted by *Swift* [1984] from *Worthington and Wright* [1970]. NADW, North Atlantic Deep Water; LSW, Labrador Sea Water; NEADW, Northeast Atlantic Deep Water; NWABW, Northwest Atlantic Bottom Water. (Reprinted from *Swift* [1984] with kind permission from Elsevier Science Ltd., The Boulevard, Langford Lane, Kidlington, OX5 1GB, UK.)

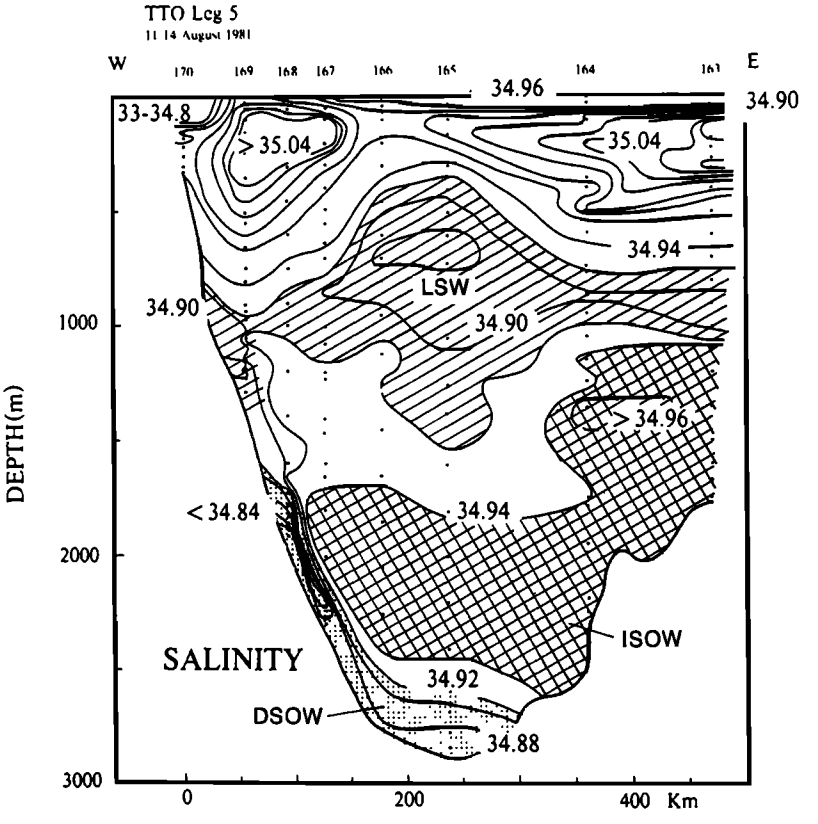

Figure 3. The vertical water mass structure in the Irminger Sea, illustrated by the TTO salinity section from East Greenland to the Reykjanes Ridge in August 1981 (from *Livingston et al.*, [1985]). Shading indicates the core of the Labrador Sea Water (LSW) layer, the Denmark Strait Overflow (DSOW) derivative, and the product of remote overflows across the Iceland-Scotland Ridge (ISOW).

Greenland Sea the relationship between the processes of deep and intermediate water production is by no means obvious; as *Aagaard and Carmack* [1989, p. 14,495] point out, we can envisage a system "in which middepth convection (which is the main source of the Denmark Strait overflow) occurs, albeit involving waters of reduced salinity, while the deeper convection which renews the deepest waters in the system is shut down."

In Figure 2, the more saline of the two overflows is the flow through the Faroe Bank Channel (labeled NEADW), which actually overflows as a relatively fresh source but mixes so intensely with warm saline water from the local thermocline that it carries a high-salinity tag thereafter, even into the western basin. The coldest and densest of the source waters in Figure 2 is the Denmark Strait Overflow (labeled NWABW), which retains its salinity minimum characteristics as it overflows and entrains, largely because of the lesser salinity difference between this overflow and its overlying waters and the increasing influence of the relatively fresh Labrador Sea Water in the entrainment/mixing process.

The fourth main constituent implied in Figure 2 is the Antarctic Bottom Water derivative represented in potential temperature-salinity space by the coldest, freshest classes in Figure 2. Of the 4–5 Sv of AABW which cross the equator, about half spreads north through the deepest layers of each basin (distinguishable by a high-silicate, high-nutrient, low-salinity, low-oxygen signal) and gradually warms, mixes, and shoals to transform from AABW into Lower North Atlantic Deep Water (the "Lower Deep Water" of *McCartney* [1992]) before recirculating southward.

In Figure 3 the vertical stacking of the first three components is illustrated for the Transient Tracers in the Ocean (TTO) section south of Denmark Strait [*Livingston et al.*, 1985] colinear with our TTO current meter array. Here the dense, fresh, freon maximum layer of Denmark Strait Overflow Water is blanketing the lower slope, the more saline, freon minimum waters derived from the remote Iceland-Scotland overflows are beginning to appear above that, and the fresh core of Labrador Sea Water is capping both at 700–1500 m depths. Any Lower Deep Water contribution is not separately distinguishable in Figure 3.

2. Direct Observations of the Denmark Strait Overflow

Early Current Measurements

The first attempts at direct measurement of the overflow in the Denmark Strait were made by *Worthington* [1969] over a period of 1 month in the winter of 1967. None of his moorings survived on the western slope of the strait where the coldest, fastest flows were expected, but the two moorings (only one complete record) recovered from the middle part of the Strait showed a highly energetic and variable flow of up to 143 cm s^{-1} with a mean of 21.4 cm s^{-1} at 760 m, a strong temperature signal, a dominant timescale of a few

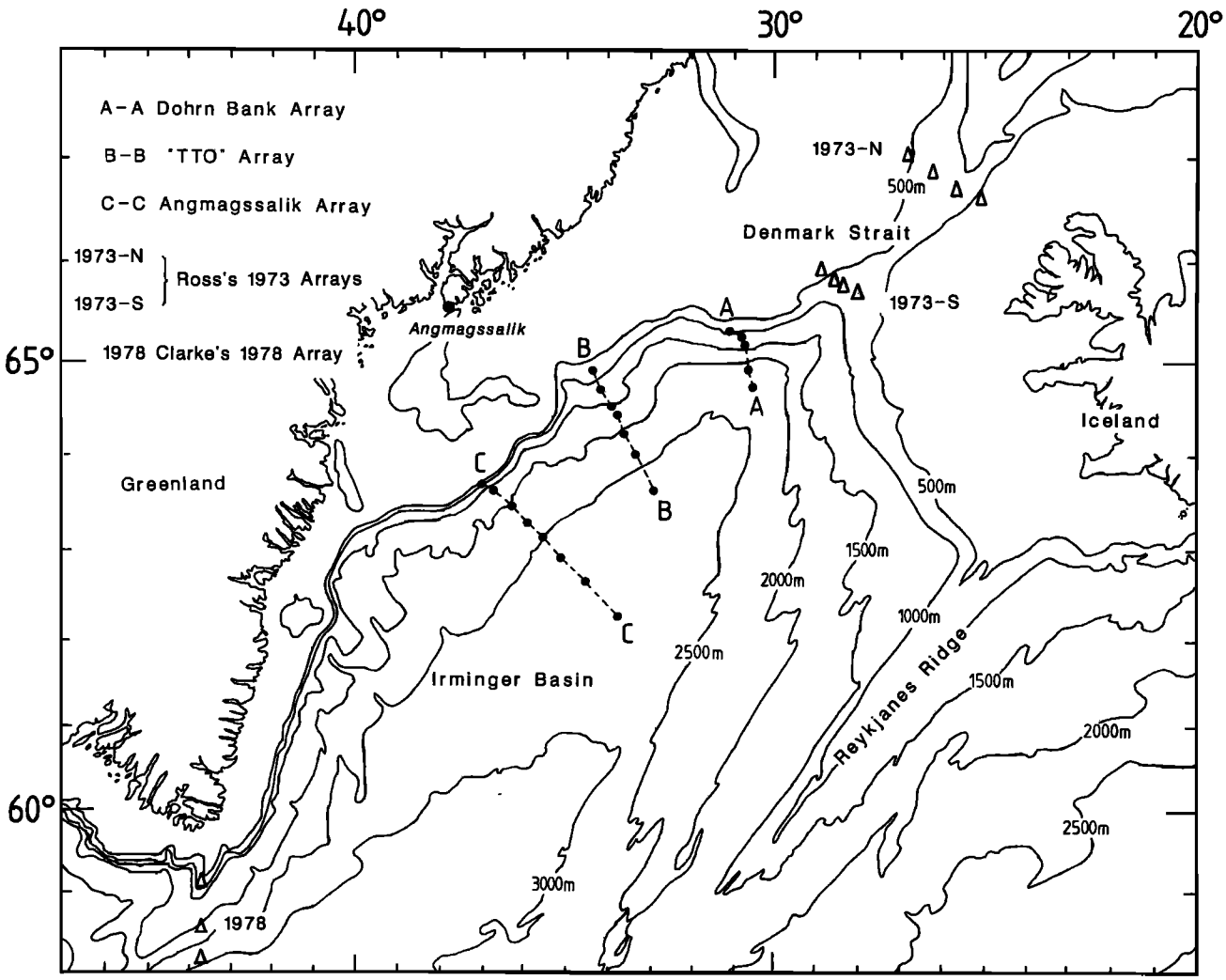

Figure 4a. Location of available long-term current meter arrays between Denmark Strait and Cape Farewell. The Dohrn Bank, TTO, and Angmagssalik arrays are those established by the Fisheries Laboratory, Lowestoft, England between 1986 and 1991.

days in both parameters, and (despite an exhaustive search) no link with atmospheric events. On the basis of the measured velocities the transport of water colder than 4°C was calculated to be 2.7 Sv.

During the International Council for the Exploration of the Sea (ICES) exercise "Overflow '73" a remarkable set of 25 five-week current records were recovered from three arrays located immediately to the north and south of the Denmark Strait sill [*Ross*, 1975, 1976, 1977, 1978, 1983, 1984]. The records from north of the sill show weak (mean <10 cm s^{-1}) and variable flows, in sharp contrast to those in the overflowing stream further south. The latter, about 55 km south of the sill (see Figure 4a), indicate a vigorous bottom-intensified flow following topography, with the core of the current (mean, >60 cm s^{-1}; maximum, 167 cm s^{-1}) lying midway up the slope on the Greenland side and with an energetic dominant fluctuation timescale of 1.8 days in both temperature and velocity present in all records and coherent in both the vertical and horizontal. *Smith* [1976] explains these observations not in terms of meteorological forcing but in terms of the steady movement of dense water south toward the strait from an upstream reservoir of constant pressure head that intensifies as it is funneled through the strait, becomes unstable hydrodynamically, and acquires its energetic fluctuating component through the development of baroclinic instability south of the sill. *Ross* [1984] estimates the time-averaged volume flux of water colder than 2°C to be 2.9 Sv.

In 1975 the first year-long records were obtained from the overflow with the recovery of moorings MONA 5 and 6 by *Aagaard and Malmberg* [1978] from the exit of the strait along 30°40'W, slightly downstream from *Ross*'s [1975] main array. Each mooring carried two instruments at heights of 25 and 100 m above the bed and all gave full 360-day records. These records confirmed Ross's observations by showing a strong bottom-intensified flow directed along the isobaths with a mean speed of about 50 cm s^{-1} and with various low-frequency variations superimposed, including a dominant and persistent fluctuation at 1.5–2.5 days, with an amplitude comparable to the mean, which *Aagaard and Malmberg* [1978] attributed (probably) to baroclinic instability. However, for the first time, these records were long

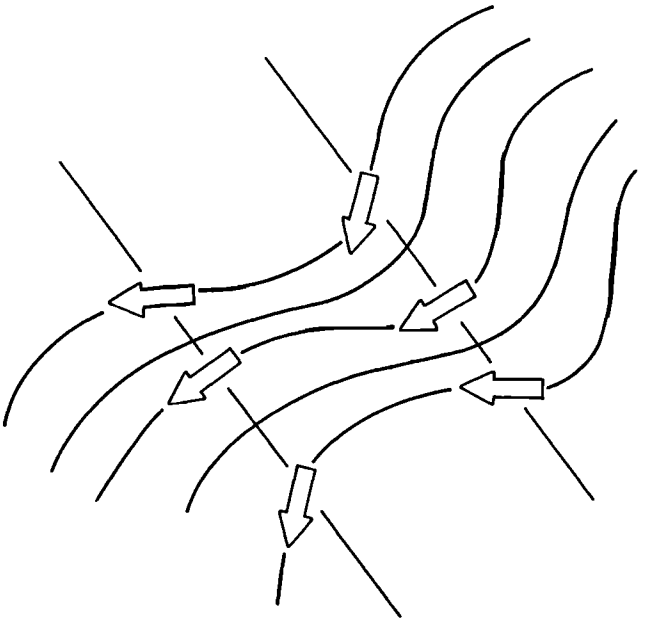

Figure 4b. Schematic diagram illustrating the variability of longslope flow direction in dissected topography.

enough to demonstrate the lack of a seasonal fluctuation in either the speed or the temperature of the overflow.

The final group of early current measurements available to us from the overflowing stream are the three moorings (six current meters) deployed south of Cape Farewell in February–April 1978 whose characteristics are reported by *Clarke* [1984] (for locations see Figure 4a). By using these 60-day means to provide a reference for his geostrophic calculations, Clarke shows that the overflow rounds Cape Farewell as a steady, bottom-trapped current lying against the lower part of the Greenland Slope in the 1900–3000 m depth range that has core speeds of >25 cm s^{-1}. Clarke's estimate of overflow transport will be discussed in section 3 below.

All of the early records described above were obtained using the Aanderaa current meter or, in the case of *Worthington*'s [1969] only complete record, using the Bergen current meter which was its prototype.

The Lowestoft Arrays, 1986–1991

Between September 1986 and August 1991, a total of 91 out of 96 current meters (Aanderaa Mk 4, 5, or 7) were recovered from the overflow by the Fisheries Laboratory, Lowestoft, England, following long-period deployments. These instruments were laid on three arrays set normal to the Greenland Slope at increasing distances from the Denmark Strait (see Figure 4a), with the specific aim of measuring the downstream changes in speed, transport, and entrainment associated with this current. To minimize knockdown in such vigorous flow conditions, these moorings were specially designed variants of the normal Lowestoft type of single-point near-bottom mooring [see *Jones and Read*, 1993]. These were short (200–1100 m in total length), with increased buoyancy (320–460 kg) and anchor weight (820–1000 kg) to increase the mooring's tautness and used 10-mm-diameter Kevlar cable of 4.5 t breaking strain to minimize drag.

Mooring details and low-passed flow statistics are listed in Tables 1 and 2. In these it is important to note that the coordinate system used is not the conventional one, where u and v refer to east and north components respectively. Instead, since the aim is to focus on the along-slope flow and its fluctuations, the coordinate system has been rotated so that u and v refer to flow in the along-slope and cross-slope directions, respectively and are used as such throughout this report. Such a procedure is common in the literature, but whereas components are normally rotated to a fixed regional orientation of slope, the special circumstances off east Greenland force a departure from convention. There the slope is so dissected by canyons that there is no common slope alignment that would be appropriate for all moorings, even those of a single array. Figure 4b schematically illustrates the point that in a topography of spurs and reentrants the true orientation of the along-slope flow component can easily differ by 90° or more between moorings, and even the generalized contour lines of Figure 4a will confirm that this point is hardly exaggerated off east Greenland. (For greater detail, see General Bathymetric Chart of the Oceans chart 5.04.) The obvious conclusion is that the true along-slope flow component can only properly be assessed in this area if we allow our coordinate system to vary according to the local topography around each mooring. Since bathymetric charts are insufficiently controlled for this purpose, we have taken the view that the best guide to the local orientation of the slope is provided by the flows themselves, since these are for the most part strong, steady and sufficiently unambiguous in direction to suggest that they are following topography. Thus in Table 2 the orientation of u is not fixed but is allowed to vary according to the long-term mean flow direction, and the listing for long-term mean speed is the along-slope flow component. In practice a glance at the mean directions column of Table 2 will confirm that within each array there is a sufficient variation in flow directions to suggest that this approach does provide a worthwhile gain in the assessment of the true along-slope component of flow for each record and in the integration of these into an along-

Table 1. Dates and Duration of Lowestoft Arrays off East Greenland, 1986–1991

Array	Laid	Recovered	Duration, days	Mooring Numbers
Angmagssalik Trial	Sept. 9, 1986	June 26, 1987	276	8606-07
Angmagssalik I	June 26–28, 1987	June 30–July 1, 1988	353–357	8701-08
Angmagssalik II	July 3–5, 1988	June 28–29, 1989	344–347	8801-08
Angmagssalik III	July 2–4 1989	Mar. 6–8, 1990 and Aug. 12, 1990	232–233 385	8906-11
Dohrn Bank	Mar 9, 1990	July 10, 1990	108–109	9001-05
TTO	July 12, 1990	July 30, 1991	368	9006-11

Table 2. Low-Pass Filtered Flow Statistics for all Deployments of the Lowestoft Current Meter Arrays in East Greenland

ID	Z, m	°N Latitude, °W Longitude	Instrument	Depth, m	Duration, days	Mean Speed, cm s^{-1}	Mean Direction, deg	$\overline{u'v'}$, cm^2 s^{-2}	$\overline{u'T'}$, cm s^{-1} °C	$\overline{v'T'}$, cm s^{-1} °C	$\bar{T}$, °C	K_E, cm^2 s^{-2}	K_M, cm^2 s^{-2}	Comments
8606		62°53.7′	8606-1	1980	276	4.42	259	−1.16	0.004	0.007	3.37	59.63	9.80	
	2640	35°51.5′	8606-2	2530	276	9.99	248	−2.93	0.071	0.452	1.74	57.55	49.91	
8607		63°25.8′	8607-1	1536	275	5.67	269	2.53	0.059	0.558	3.15	168.82	16.06	
	2046	36°34.2′	8607-2	1936	276	20.33	262	−8.15	2.180	−0.324	2.01	132.66	206.75	
8701		63°42.4′	8701-1	919	357	22.88	238	−13.93	0.115	−0.089	3.76	84.12	261.67	
	1220	36°58.3′	8701-2	1120	357	25.98	241	−2.78	−0.108	−0.064	3.54	81.21	337.54	
8702		63°36.3′	8702-1	1247	85	29.41	227	17.77	1.755	0.040	3.32	114.81	432.53	Temps 59 days.
	1648	37°1.9′	8702-2	1548	356	25.39	233	−3.61	0.712	−0.128	2.77	55.57	322.40	
8703		63°29.1′	8703-1	1585	356	9.42	251	−3.15	0.822	0.511	3.08	184.20	44.36	
	1986	36°17.4′	8703-2	1886	356						1.92			Meter fouled, temperatures only.
8704		63°16.7′	8704-1	1754	355	4.88	235	−14.49	−0.112	0.128	3.38	90.15	11.92	
	2355	35°53.6′	8704-2	2255	355	22.25	244	−0.33	0.774	0.905	1.65	127.07	247.47	
8705		63°7.0′	8705-1	1869	355	2.73	252	−3.02	−0.104	−0.100	3.40	64.88	3.72	
	2572	35°33.3′	8705-2	2472	355	11.84	236	−12.82	−0.008	0.544	1.67	85.16	70.15	
8706		62°54.1′	8706-1	1903	354	1.49	71	−8.60	0.002	−0.027	3.39	27.70	1.11	
	2706	35°6.4′	8706-2	2606	257	1.52	251	−19.57	−0.792	0.684	1.84	61.24	1.15	Split record. Mean temperature for 354 day series = 1.85°C.
8707		62°38.4′	8707-1	2032	278	1.96	265	3.67	0.004	−0.019	3.36	16.29	1.91	Split record.
	2835	34°30.4′	8707-2	2735	353	3.20	240	−4.13	−0.458	0.044	1.98	24.63	5.12	
8708		62°15.4′	Lost	2013										Lost.
	2916	33°48.6′	Lost	2816										Lost.
8801		63°28.9′	8801-1	1622	279	12.30	257	24.67	0.792	0.679	2.88	230.00	75.63	
	1984	36°17.9′	8801-2	1924	204	24.67	260	−9.12	1.762	−0.765	1.71	141.62	304.31	Split record. Mean temperature for 347 day series = 1.65°C.
			8801-3	1965	347	26.27	250	−8.95	0.847	−0.935	1.57	131.63	345.00	
8802		63°37.2′	8802-1	1298	347	26.70	242	40.01	3.510	0.213	2.95	203.30	356.10	
	1660	36°43.8′	8802-2	1600										Meter malfunction.
			8802-3	1641	214	25.69	230	14.55	0.644	−1.051	2.19	96.03	329.92	Mean temperature for 347 day series = 2.07°C.
8803		63°41.7′	8803-1	998	228	30.23	253	−47.32	0.857	−0.378	3.74	142.11	456.98	Suspect directions at high speeds.
	1260	36°59.2′												
			8803-2	1200										Battery failed; no data.
			8803-3	1241	347	23.69	234	−1.75	0.639	−0.100	3.22	38.80	280.58	
8804		63°16.7′	8804-1	1733	346	4.64	221	−40.99	−0.023	0.159	3.34	139.66	10.77	Directions suspect.
	2345	35°52.2′	8804-2	2285	39	22.00	242	−10.73	0.812	−0.659	1.24	105.75	241.86	
			8804-3	2326	266	24.03	243	−8.80	0.444	−0.320	1.31	119.30	288.84	Temperatures 13 days.
8805		63°7.1′	8805-1	1895	128	2.24	275	14.32	0.023	−0.016	3.38	76.87	2.51	Split record. Mean temperature for 327 day series = 3.36°C.
	2569	35°32.5′												
			8805-2	2509	346	13.18	238	−6.20	0.470	0.540	1.26	111.46	86.81	
			8805-3	2550										Battery failed; no data.

Table 2. (continued)

ID	Z, m	°N Latitude, °W Longitude	Instrument	Depth, m	Duration, days	Mean Speed, cm s^{-1}	Mean Direction, deg	$\overline{u'v'}$, cm^2 s^{-2}	$\overline{u'T'}$, cm s^{-1} °C	$\overline{v'T'}$, cm s^{-1} °C	$\overline{T}$, °C	K_E, cm^2 s^{-2}	K_M, cm^2 s^{-2}	Comments
8806		62°54.4′	8806-1	1871	345	1.78	281	8.69	−0.015	−0.018	3.37	34.08	1.58	
	2706	35°6.6′	8806-2	2646	345	6.25	256	−4.32	−0.274	0.292	1.37	49.21	19.56	
			8806-3	2687	63	7.20	268	2.62	0.273	−0.107	1.10	50.87	25.93	
8807		62°39.2′	8807-1	2052	345	1.47	184	2.07	−0.041	0.026	3.35	30.64	1.08	
	2827	34°30.9′	8807-2	2767	345	4.83	196	−1.49	0.210	0.228	1.36	48.21	11.66	
			8807-3	2808	345	5.63	213	−9.28	0.013	0.133	0.94	52.42	15.86	Temperatures 61 days.
8808*		62°14.2′	8808-1	2042	201	5.18	77	0.42	−0.049	0.037	3.39	38.67	13.39	
	2917	33°48.6′	8808-2	2857	250	2.53	97	−5.19	0.355	−0.020	1.55	46.67	3.20	Temperatures 63 days. Series has some suspect directions.
					115	2.88	120	4.42	0.355	−0.020	1.55	53.26	4.14	Temperatures 63 days.
			8808-3	2898	344	3.39	110	−4.57	−0.083	0.628	1.21	53.42	5.73	
8906		62°47.0′	8906-1	2431	232	0.41	183	6.00	−0.024	0.023	2.94	21.33	0.09	
	2756	34°48.1′	8906-2	2693										Meter malfunction.
			8906-3	2736	119	6.51	245	−9.06	0.181	0.480	1.10	38.62	21.19	Temperatures 58 days.
8907		63°00.0′	8907-1	2229	233	3.50	283	−4.32	0.027	0.006	3.05	38.04	6.12	
	2634	35°20.1′	8907-2	2571	233	9.05	272	−12.31	−0.269	−0.065	1.42	51.84	40.93	
			8907-3	2614	233	11.05	269	−8.57	0.117	−0.151	1.07	51.58	61.04	
8908		63°12.1′	8908-1	2026	385	4.19	232	−27.88	−0.162	0.236	3.20	95.01	8.78	
	2463	35°43.7′	8908-2	2400										Meter leaked.
			8908-3	2443	97	21.16	238	−30.76	0.341	−0.162	1.05	85.85	223.92	
8909		63°23.0′	8909-1	1788	232	11.72	257	−21.38	−0.940	0.841	2.91	184.82	68.61	
	2153	36°5.3′	8909-2	2090	232	24.53	254	−19.21	1.444	−0.427	1.46	137.18	300.89	
			8909-3	2133	141	24.17	249	−15.56	0.509	−0.283	1.35	118.98	292.10	Split record. Temperatures 29 days only.
8910		63°33.4′	8910-1	1402	233	12.72	245	−20.50	1.146	0.190	2.97	243.12	80.85	
	1767	36°30.3′	8910-2	1704	51	26.49	253	−30.56	1.302	−0.184	2.04	129.35	350.97	
			8910-3	1747	107	26.96	245	−22.79	1.463	−0.214	1.85	94.70	363.44	
8911		63°39.4′	8911-1	1180	49	30.47	230	39.68	2.706	0.566	3.11	204.60	464.09	
	1445	36°51.5′	8911-2	1382	232	34.62	220	3.84	2.416	0.192	2.63	63.88	599.46	
			8911-3	1425	32	31.90	211	3.98	1.885	0.003	2.63	33.20	508.65	
9001		64°45.0′	9001-1	1198	109	1.60	271	3.16	−0.462	−0.173	3.73	34.22	1.28	
	2200	30°33.0′	9001-2	1679	108						3.53			Meter fouled; temperatures only.
			9001-3	2180	109	5.36	288	8.11	−0.375	0.040	2.94	53.84	14.35	
9002		64°54.8′	9002-1	1155	108	1.45	305	0.20	−0.076	−0.115	3.70	45.46	1.05	
	2005	30°40.1′	9002-2	1906	88	4.61	270	13.59	0.740	0.414	3.43	107.05	10.65	Mean temperature for 108 day series = 3.43°C.
			9002-3	1987	108	21.68	262	84.74	9.363	4.932	2.27	190.35	235.16	
9003		65°9.9′	9003-1	880	109	7.12	271	−51.29	−0.952	−0.232	4.17	183.14	25.34	
	1500	30°47.0′	9003-2	1231	109	12.44	260	−26.36	5.610	3.103	2.64	190.85	77.33	Some suspect speeds.
					41	20.79	259	−90.88	5.827	4.291	2.61	299.16	216.11	Split record.†
			9003-3	1482	109	51.14	260	9.77	1.237	1.148	0.96	163.25	1307.45	

Table 2. (continued)

ID	Z, m	°N Latitude, °W Longitude	Instrument	Depth, m	Duration, days	Mean Speed, cm s^{-1}	Mean Direction, deg	$\overline{u'v'}$, cm^2 s^{-2}	$\overline{u'T'}$, cm s^{-1} °C	$\overline{v'T'}$, cm s^{-1} °C	$\overline{T}$, °C	K_E, cm^2 s^{-2}	K_M, cm^2 s^{-2}	Comments
9004		65°15.3′	9004-1	750	109	11.08	274	−61.98	−0.764	3.132	4.20	334.79	61.38	
	1200	30°50.9′	9004-2	1101										Meter leaked.
			9004-3	1182	109	48.65	259	−26.03	0.456	0.190	1.06	104.19	1183.31	
9005		65°17.9′	9005-1	680	109	14.65	287	−75.55	3.230	1.687	4.14	394.13	107.29	
	1080	31°6.9′	9005-2	981	23	45.92	277	−26.22	10.236	1.070	1.83	253.65	1054.45	
			9005-3	1062	109	46.37	265	1.77	1.178	0.379	1.34	123.08	1075.26	
9006‡		63°37.3′	9006-1	1634	370						3.30			Meter fouled; temperatures only.
	2738	32°55.6′	9006-2	2136	370	2.97	3	−10.38	0.107	−0.078	3.35	45.82	4.42	Temperatures 7 days.
			9006-3	2638	351	1.62	349	−22.32	−0.598	−0.120	2.28	77.26	1.31	
			9006-4	2720	43	2.66	194	−14.77	−0.504	0.516	1.22	42.76	3.54	
9007		64°1.9′	9007-1	1523	Lost									Lost.
	2345	33°21.2′	9007-2	2285	Lost									Lost.
			9007-3	2327	Lost									Lost.
9008		64°16.3′	9008-1	1249	355						3.46			No Speeds.
	2001	33°37.8′	9008-2	1631	358						3.34			No Speeds.
			9008-3	1983	318	27.37	235	5.72	1.294	1.366	1.11	177.98	374.68	Temperatures 104 days.
9009		64°25.8′	9009-1	1529	368	9.55	245	−29.70	1.363	1.946	2.80	288.43	45.53	Temperatures 222 days.
	1731	33°46.8′	9009-2	1671	15	31.61	245	−47.53	0.247	1.148	1.57	131.10	499.56	Temperatures 368 days.
			9009-3	1713	87	33.48	236	−25.48	1.252	−0.096	0.89	216.50	560.38	
9010		64°33.0′	9010-1	992	357	9.18	244	−74.18	0.976	0.049	3.43	422.84	42.18	
	1494	33°55.6′	9010-2	1394	353	25.59	249	−26.87	4.416	1.169	2.02	280.80	327.26	
			9010-3	1476	368	29.18	240	−20.27	1.101	−0.712	1.49	178.44	425.65	
9011		64°43.2′	9011-1	940	368	18.23	250	−6.76	1.737	0.133	3.14	286.41	166.19	
	1142	34°6.3′	9011-2	1082										Meter malfunction.
			9011-3	1124	368	26.00	241	0.13	0.418	−1.490	1.76	156.96	337.19	Noisy temperatures.

The Hilow filter of *Cartwright* [1983] is used throughout. T is temperature.

*For calculating statistics based on along-slope (u) and cross-slope (v) flows, slope orientation for mooring 8808 is assumed to be 33°/213°. For this reorientation the along-slope flow is as follows: 8801-1, 3.71 cm s^{-1} at 33°; 8808-2, 0.15 cm s^{-1} at 33°; and 8808-3, 0.76 cm s^{-1} at 33°.

†Note that statistics from the shorter (41 day) series were used in Figures 8, 9, and 11.

‡For calculating statistics based on along-slope (u) and cross-slope (v) flows, slope orientation for mooring 9006 is assumed to be 55°/235°. For this reorientation the along-slope flow is as follows: 9006-1, 1.83 cm s^{-1} at 55°; 9006-2, 0.66 cm s^{-1} at 55°; and 9006-3, 2.01 cm s^{-1} at 235°.

slope transport estimate. In only two cases does the procedure not work. These are the cases of the easternmost moorings of the Angmagssalik and TTO arrays (moorings 8808 and 9006, respectively) which lie so far offshore that they no longer "feel" the slope or participate in the overflow. From the viewpoint of calculating the along-slope transport, it matters little how we treat these moorings; their flows are weak and do not contribute to the along-slope southward transport [five out of six records are directed to the north and east]. However, for consistency we have recalculated the along-slope components of flow for these records using assumed orientations of the local slope (these recalculated speeds are listed as footnotes in Table 2 and are the values used in the along-slope speed plots shown in Figure 11).

Since Table 2 not infrequently refers to a split record, Figure 5a provides an example in the form of a 200 day low-passed segment from instrument 8805-1. Although the instrument appears to work normally for most of the time, there is an obvious temporary failure of the speed sensor for a period of 30 days in midrecord from an unknown cause. It would plainly be wasteful of data merely to discard the record from the time of the failure and, providing the bad portion is discarded, the use of the remainder makes little difference to the statistics compiled in Table 2, since these are simply based on means and deviations from means. Periodicity analysis would obviously require some gap-filling technique, however.

The historical record of direct current measurements is therefore becoming quite extensive. However, the question of variability at a range of timescales must be addressed before 5- and 50-week records can be compared to assess any downstream change in flow conditions, or even before our year-long records from different settings of the Angmagssalik array can be plotted together to form a reliable transport estimate. Since these are our principal aims, the question of variability is described in some detail below.

Temporal Variability

In any given record from the core of the current, the histograms of current speed and direction provide evidence of a strong, steady, well-defined flow with few subthreshold speeds (e.g., Figures 5b–5e).

Energetic variability at periods of a few days. Though concealed in the types of data presentation given in Figure 5, our near-bottom records agree with all previous records from the core of the overflow in showing a characteristic large-amplitude dominant fluctuation in current speed with a period of a few (typically 1–12) days and an amplitude similar to that of the mean. However, care must be taken in defining the domain of this dominant fluctuation timescale since it is far from ubiquitous.

If we compare eight contemporaneous 347-day near-bottom low-passed current records from the 1988–1989 deployment of the Angmagssalik array in order to examine the extent of this fluctuation in the near-bottom layer (Figure 6), we find that it is best developed in the depth zone occupied by the core of the current (top four panels in Figure 6). There the dominant fluctuations are of a higher frequency and a larger amplitude and that frequency and amplitude are more consistent in time than is the case for records from the lower fringes of the current farther down the slope (lower four panels in Figure 6). A similar pattern of behavior can be shown to characterize the temperature fluctuations across this slope, as illustrated in Figure 7 using seven contemporaneous 1-year series from the earlier 1987 deployment of this array.

Figures 8 and 9, however, describe the distributions of eddy kinetic energy (K_E) and the kinetic energy of the mean flow (K_M) per unit mass, respectively, on the three main instrumented arrays. Definitions are conventional:

$$K_M = \tfrac{1}{2}\,[\bar{u}^2 + \bar{v}^2]$$

$$K_E = \tfrac{1}{2}\,[\overline{u'^2} + \overline{v'^2}]$$

where $u'^2 = \sum (u - \bar{u})^2$ and $v'^2 = \sum (v - \bar{v})^2$.

From these it is clear that the fluctuation kinetic energy is not a characteristic of either the near-bottom layer or the core of the overflow but reaches its (considerable) maximum of ~400 $cm^2\ s^{-2}$ in the upper reaches of the slope, well clear of the bottom, though at a depth which deepens with distance southward from the strait (close to 500 m on the Dohrn Bank array, 1000 m on the TTO array, and 1500 m on the Angmagssalik array).

In the amplitude of the K_E and K_M maxima, in their location and apparent dissociation in space, and, especially, in the intense near-bed gradient in K_M (exceeding 4 orders of magnitude in a vertical distance of only a few hundred meters) these observations are most closely matched in the literature by the Mediterranean outflow at the Gibraltar Sill (*Pillsbury et al.* [1987] and H. L. Bryden (personal communication, 1993); see also *Dickson* [1990, Table 119]).

In the present context of long-term production rates and pathways it is neither relevant nor practicable to discuss the possible causes of this short-period signal or its distribution and coherence across the Greenland Slope. It is worth adding only that these energetic fluctuations may not be wholly dissociated from the deepening overflow plume. J. G. Bruce and L. M. Patman (U.S. Naval Oceanographic Office, personal communication, 1992) use satellite IR imagery to show that the trains of small (15–30 km diameter) cyclonic eddies have a close association with the Greenland Slope south of the Denmark Strait and that these eddies move out over slightly deeper water as they propagate south in much the same manner as the overflow plume itself. They therefore suggest that vortex stretching associated with the sinking plume might be a cause via much the same mechanism as *Whitehead et al.* [1990] demonstrate in their rotating tank models.

Record length required to form a stable mean. The key question of whether these records can be compared with other earlier recoveries, some of which are of short duration, will depend upon the length of record required to form a stable mean. In Figure 10, we estimate this using 10 representative near-bottom records recovered in four successive years from two arrays on the Greenland Slope. (The relative location of each record is shown in the inset of Figure 12.) For each instrument we calculate the mean speed over time intervals varying from one day to the full record length, in increments of one-day steps. After rapid initial fluctuations the mean speed is tolerably well established within 30 days, the exception being the deepest record of the group (8909-2) which lies outside the main core of the overflow, and where ~90 days are required for the development of a representative mean.

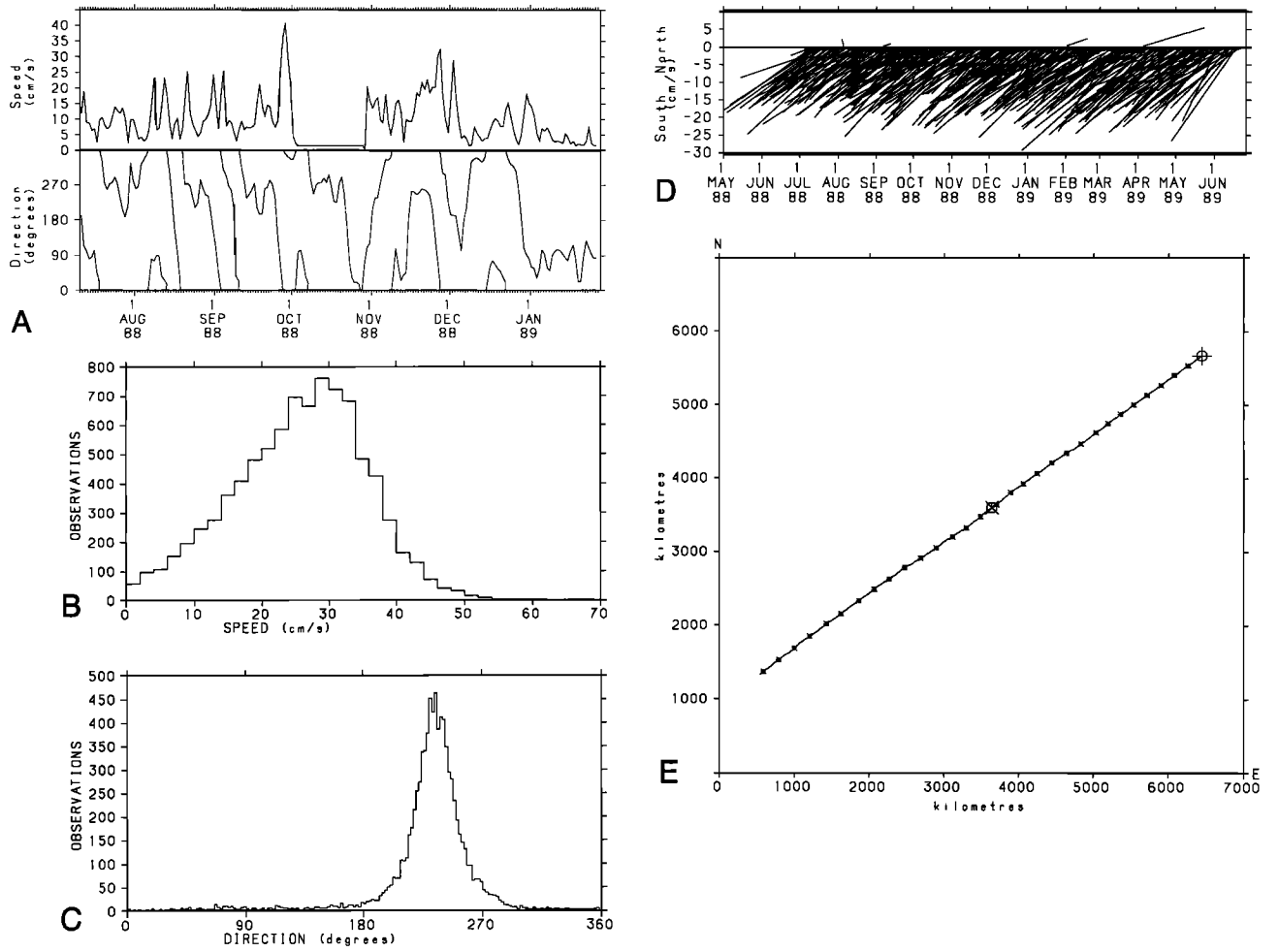

Figure 5. Extracts from current meter records from the Denmark Strait Overflow: (a) example of a split record in a 200-day segment from instrument 8805-1. The histograms of hourly values of (b) speed and (c) direction. (d) A stick plot of low-passed daily mean speed vectors, and (e) a progressive vector diagram based on vectors (ticks at 10-day intervals) for the 361-day record at instrument 8803-3. For instrument and mooring details, see Table 2. *Cartwright*'s [1983] HILOW filter is used.

Lack of seasonal variability. In the present context the next essential point to develop is the contrast between the highly energetic fluctuations with periods of a few days and the relative absence of variability at larger timescales.

Figures 6 and 7, our longest and most complete descriptions of the Denmark Strait overflow within the period of a year, provide no clear evidence of any seasonal fluctuation in either current speed or temperature. A similar conclusion will be evident in the 30-day mean speeds from the core of the overflow shown in Figure 11. This in itself is not an unexpected result. Though *Gould et al.* [1985] describe an apparent seasonal signal in the inflowing slope current west of Shetland, the outflows and their sources appear to be nonseasonal. In the Faroe Bank Channel a 1-year mooring by *Saunders* [1990] located in the cold outflow revealed the usual energetic fluctuations of a few-days period but no seasonal variation in the intensity, temperature, or thickness of the outflow (the latter observed by thermistor chain). Further downstream, where the overflow participates in the interbasin through flow via the Charlie-Gibbs Fracture Zone (CGFZ), *Saunders* [this issue] reports a lengthening of the dominant timescales to weeks or months but, again, no annual signal in the overflow could be detected. And as *Aagaard and Malmberg* [1978] have already observed, there appears to be no seasonal modulation of flow speeds in their MONA 5 and 6 records from the exit of the Denmark Strait.

Initial indications of only a weak interannual variability. While a lack of seasonality in the Denmark Strait overflow might therefore have been expected, the Lowestoft data set off East Greenland has now lengthened sufficiently to provide the first indications that its interannual variability might be equally weak; that result is certainly unexpected [*Wunsch*, 1992].

The difficulties of measurement are such that we will not easily or soon be able to strengthen this conclusion beyond its present tentative state, and even so it is certainly not intended to apply outside the period of present measurements. It is difficult in such abrupt and dissected topography as the east Greenland Slope to relocate instruments at comparable depths and locations in successive years, so that true time series longer than one deployment are strictly unobtainable. Nevertheless, when we group our available records from the overflow according to their depth range on the slope and plot speeds and directions as 30-day averages

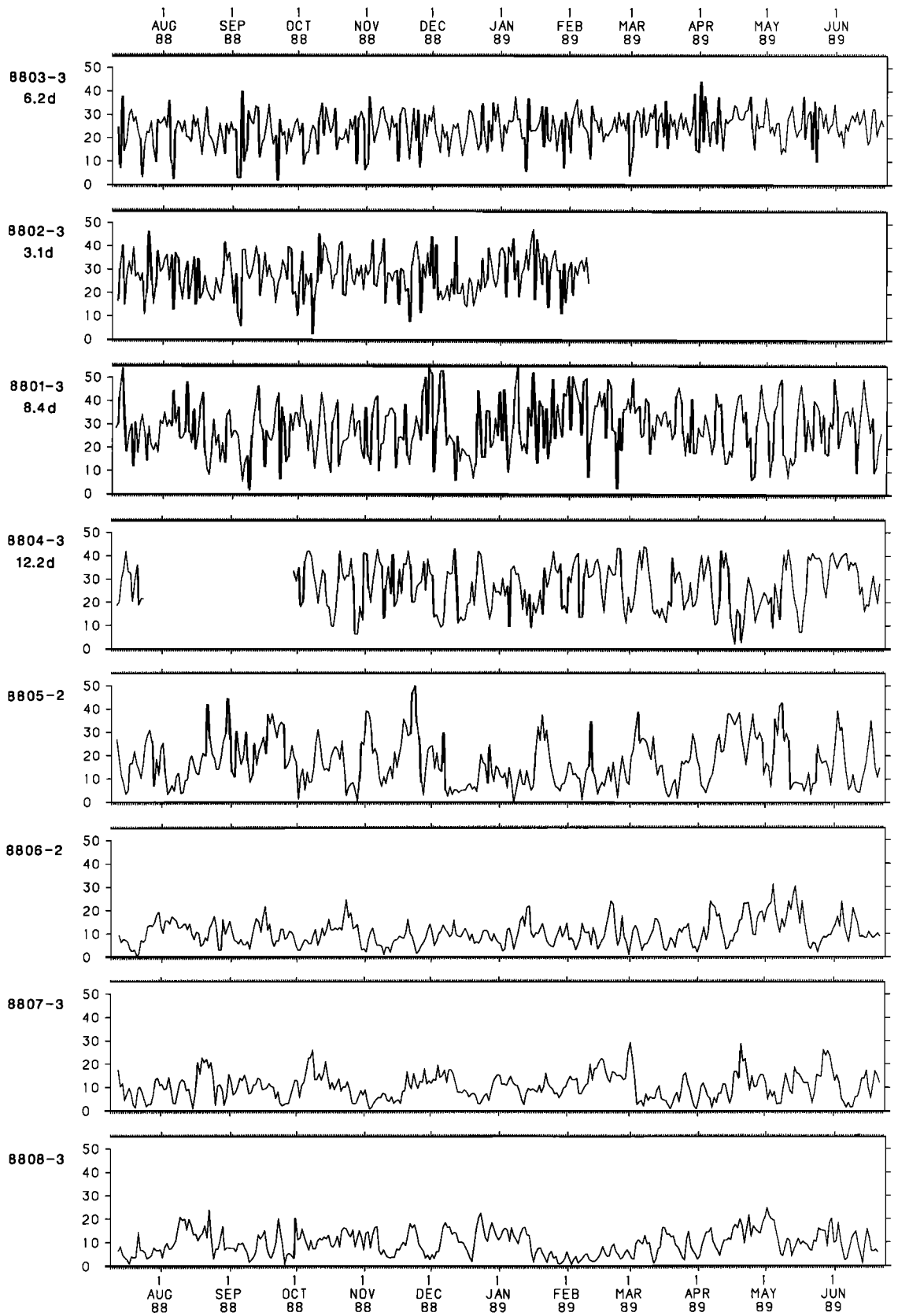

Figure 6. Time series of low-passed daily current speeds for eight contemporaneous 347-day near-bottom current records on the Angmagssalik II array across the continental slope off east Greenland (July 1988–June 1989). There is a large amplitude dominant timescale of a period of a few (3–12) days within the overflow current (top four panels) but no seasonal variation in any of the eight records. For instrument details see Table 2.

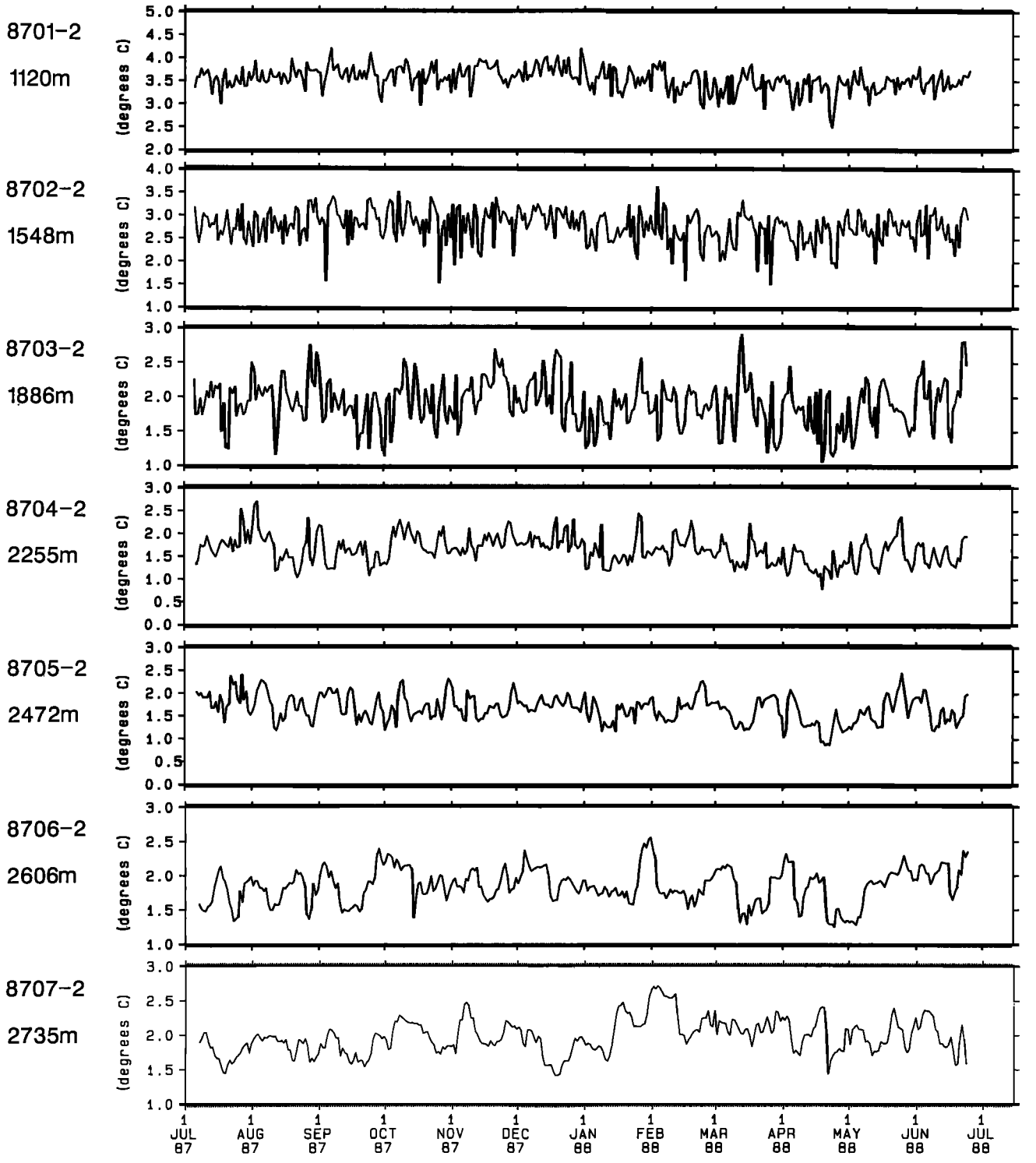

Figure 7. Time series of daily mean temperature in seven contemporaneous 357-day near-bottom current meter records from the Angmagssalik I array across the continental slope off east Greenland (June 1987–July 1988). The high-frequency variability is again greatest within the core of the overflow, and there is little evidence of any seasonal variation in any record.

to eliminate the high-frequency fluctuations, there is at least some indication in Figure 11 that means do not vary by more than a few degrees and a few centimeters per second over periods longer than a single year. In 1994 a decade of single-mooring deployments is planned to further investigate this intriguing possibility.

Whether or not these indications of flow stability prove durable in the longer term, they are already of value to the calculation of overflow transport and entrainment in two ways. First, they suggest that measurements as short as 1 month may nevertheless be representative of the overflow, so that, for example, the 5-week series obtained by *Ross*

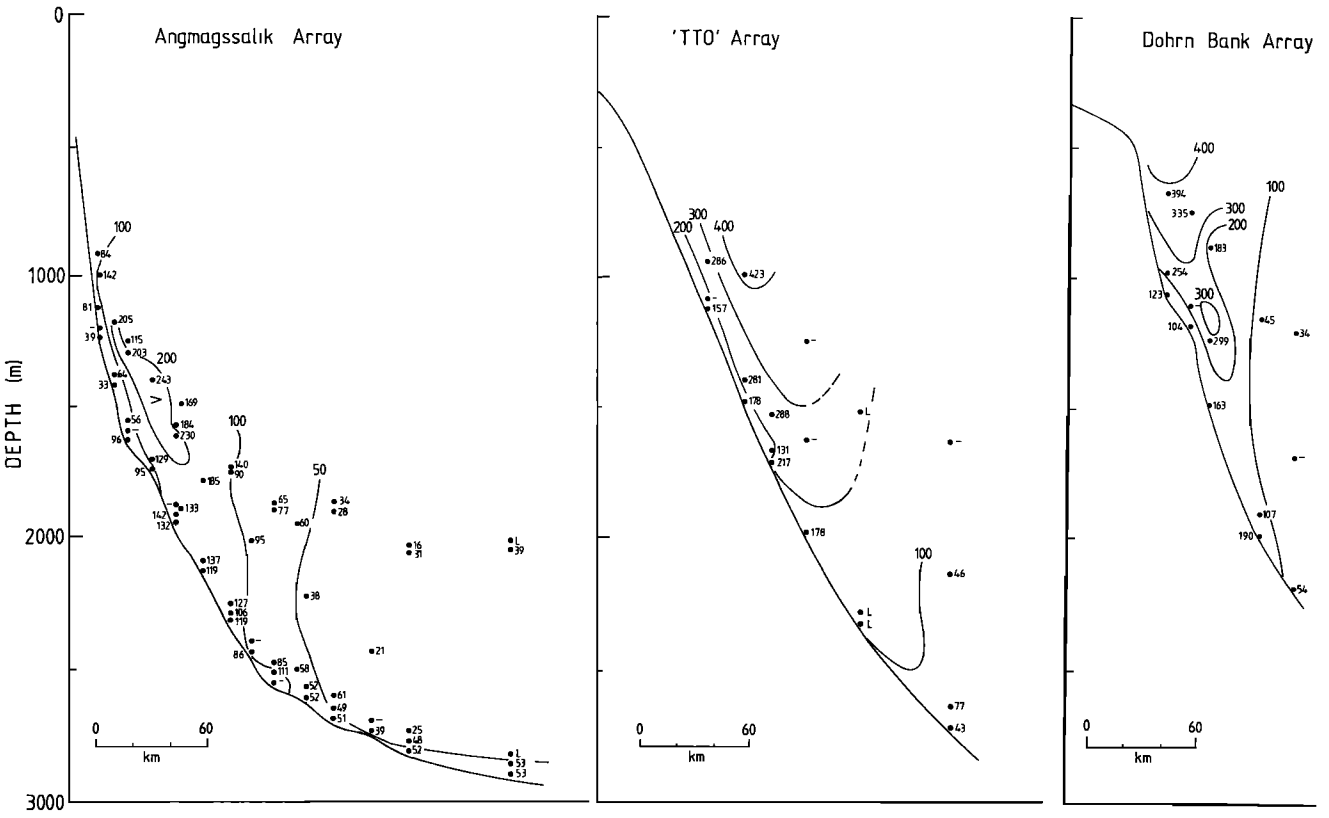

Figure 8. Distributions of eddy kinetic energy per unit mass ($cm^2\ s^{-2}$) on the Dohrn Bank, TTO, and Angmagssalik arrays. The Angmagssalik plot is a composite of results from all four deployments.

[1975] in 1973 may be comparable with our year-long series off Angmagssalik. Second, they suggest that on the Angmagssalik section, current meter data from different annual deployments may be plotted together to form a single detailed transect of flow speeds. We make use of both of these points in the comparisons which follow.

The Spatial Variation in the Depth and Speed of the Overflow From Denmark Strait to Cape Farewell

The five panels of Figure 12 illustrate the downstream evolution of the speed and depth of the overflow south of Denmark Strait, based on all available evidence and, with the exception of the Cape Farewell panel, to a common scale. Though from different years and of very different durations, the relative steadiness of the flow for periods longer than about 1 month (see above) gives some grounds for the belief that speeds may be compared, and we have no reason to suppose that the changing depth zones occupied by the current as it flows south are anything but typical. Figure 12 makes two clear points. First, it shows that the initial deceleration of the current from a peak of >60 cm s^{-1} just south of Denmark Strait to 33 cm s^{-1} on the TTO array is much more rapid than its subsequent deceleration through the Angmagssalik array to Cape Farewell (25–30 cm s^{-1} peak mean speeds throughout). Second, the rate of deepening of the core of the current is also a nonlinear function of distance downstream, deepening at a rate of 600 m/100 km between Denmark Strait and Dohrn Bank, but at a rate of only 100 m/100 km between the TTO and Angmagssalik arrays.

In one of the earliest investigations of overflow dynamics, *Bowden* [1960] identified bottom friction as the mechanism responsible for disrupting geostrophy and for directing the flow across bottom contours. He cites contour-crossing angles of 5°–6° for the deep southward flow off southeast Greenland (Cape Dan and Cape Farewell). Later stream tube models by *Smith* [1975], *Baringer and Price* [1990], and *Price et al.* [1993] augment the bottom friction term with a retardation due to the entrainment of the relatively quiescent and buoyant resident watermass. It is in the initial descent of the slope, where the largest flows are found, that the contribution of entrainment is most influential, rapidly increasing the cross-sectional area of the flow and adding to the decelerating effect of bottom friction.

As a result the contour-crossing angle is greater than for bottom friction alone. Calculating this angle from the interarray distance divided by the true downslope excursion (in kilometers) in making good the observed descent (arrowed in Figure 12) we obtain values of 18°, 5°, and 4° between the 1973-S array of *Ross* [1975] and Dohrn Bank, Dohrn Bank and TTO, and TTO and Angmagssalik, respectively (locations shown in Figure 4). Though the angles for the initial deepening of the plume are smaller than those calculated and simulated by *Smith* [1975] on the basis of short-term hydrography, all three estimates (*Bowden* [1960], *Smith* [1975], and the present study) converge on a value of ~5° south of the TTO array, suggesting the dominance of bottom friction as a control on deepening rate from this point south.

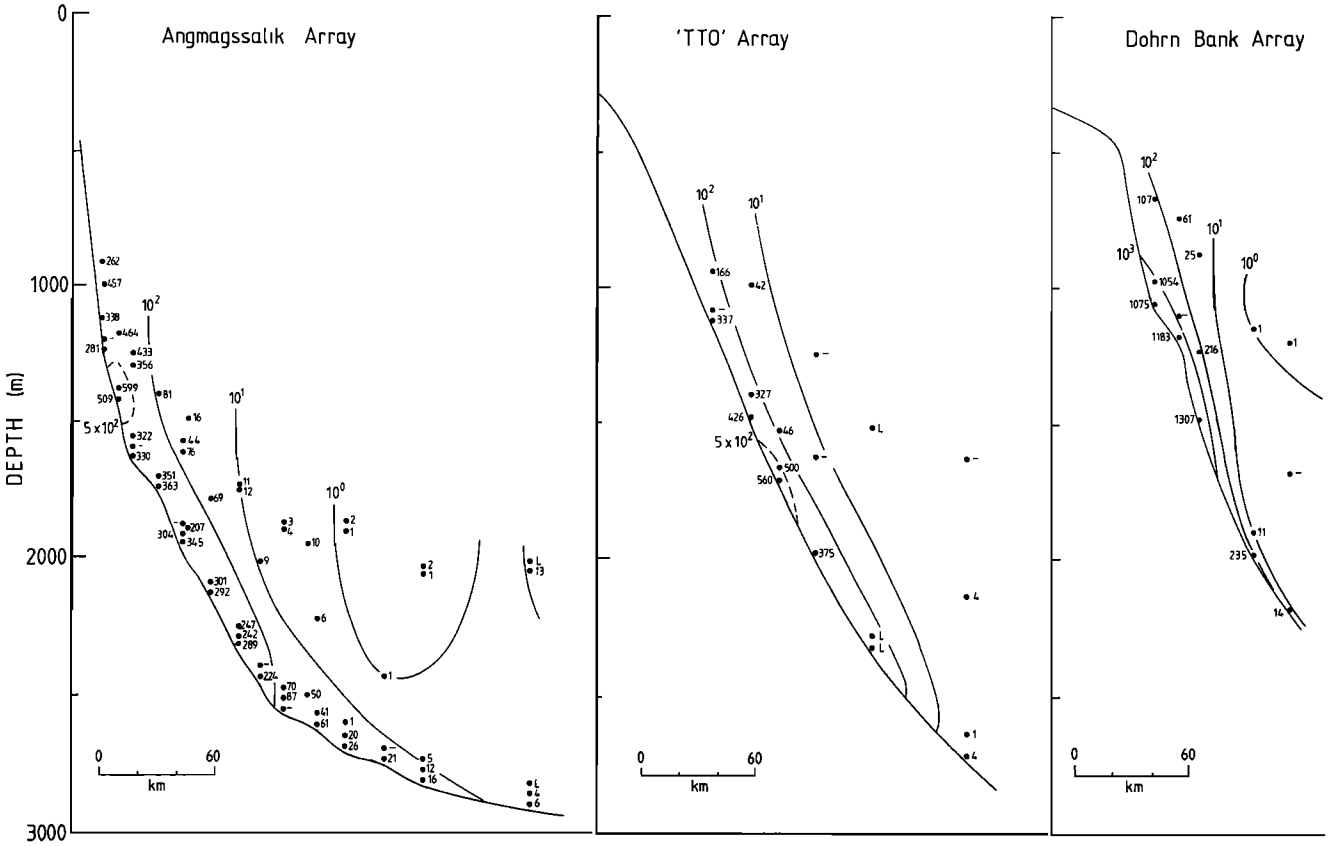

Figure 9. Distributions of the kinetic energy of the mean flow per unit mass ($cm^2\ s^{-2}$) on the Dohrn Bank, TTO, and Angmagssalik arrays. The Angmagssalik plot is a composite of results from all four deployments.

3. Sources and Pathways

This section attempts the task of piecing together a dense water transport scheme for the northern gyre from the available direct and indirect evidence and, where possible, of providing some information on its likely reliability.

Since the intention is not merely to include the waters of the Denmark Strait Overflow ($\sigma\theta$ = 27.95 − 28.0 [*Swift et al.*, 1980]) or of the Iceland-Scotland Overflows but also to include the water masses with which they might entrain or merge in forming North Atlantic Deep Water, the density range selected for these transport estimates was intentionally set rather broad to cover the full range of potential densities ($\sigma\theta > 27.8$) discussed and described by *Swift et al.* [1980].

Though this choice might certainly be objected to on the grounds that it is perhaps a little too broad, including as it does the lower part of a recirculating Labrador Sea Water layer in the northwest Atlantic [*McCartney*, 1992], it is difficult to select an isopycnal range which would be ideal everywhere for our purpose. It does at least err on the side of inclusion rather than on the exclusion of key components of overflow or their cold and warm water entrainments. The intense isopycnal gradients capping the cold, dense, near-bottom layer at the points of overflow mean that it is as good a choice as any for these sites, and it does cover a density range for which dense water transport estimates have recently been published by others (e.g., *Saunders'* [this issue] estimate for the CGFZ throughflow).

The dense water transport scheme for the northern gyre described in Figure 13 is discussed below according to its principal routes and pathways: first the "northwestern stream" from the Denmark Strait to Cape Farewell, second the "northeastern stream" from the Faroe Bank Channel to the CGFZ throughflow, and third the other less quantifiable contributions required to balance the budget where these two streams merge.

The Northwestern Stream

Our account of dense water flux along this pathway begins with the Denmark Strait Overflow itself, and here we have a range of converging estimates to support the contention that the present-day value for this throughflow is now reasonably well known. First, B. Rudels and D. Quadfasel (unpublished manuscript, 1993) demonstrate that of all the intermediate and deep waters formed in the Arctic Ocean and Subarctic Seas an annual total production of only 2.5 Sv of Arctic Intermediate Water plus 0.5 Sv of Upper Polar Deep Water (from the Canada Basin) are delivered southward to the Denmark Strait at depths shallow enough to overflow the sill. Second, based on his 5-week current measurements (which we now know to be sufficiently long to describe a valid mean), *Ross* [1984] set the cold water flux just south of the sill at 2.9 Sv. Third, by applying their four-end-member mixing model to the Angmagssalik Section further south, A. Watson et al. (unpublished manuscript, 1993) estimate that 2.7 Sv of the water passing through that section at $\sigma\theta \geq 27.80$

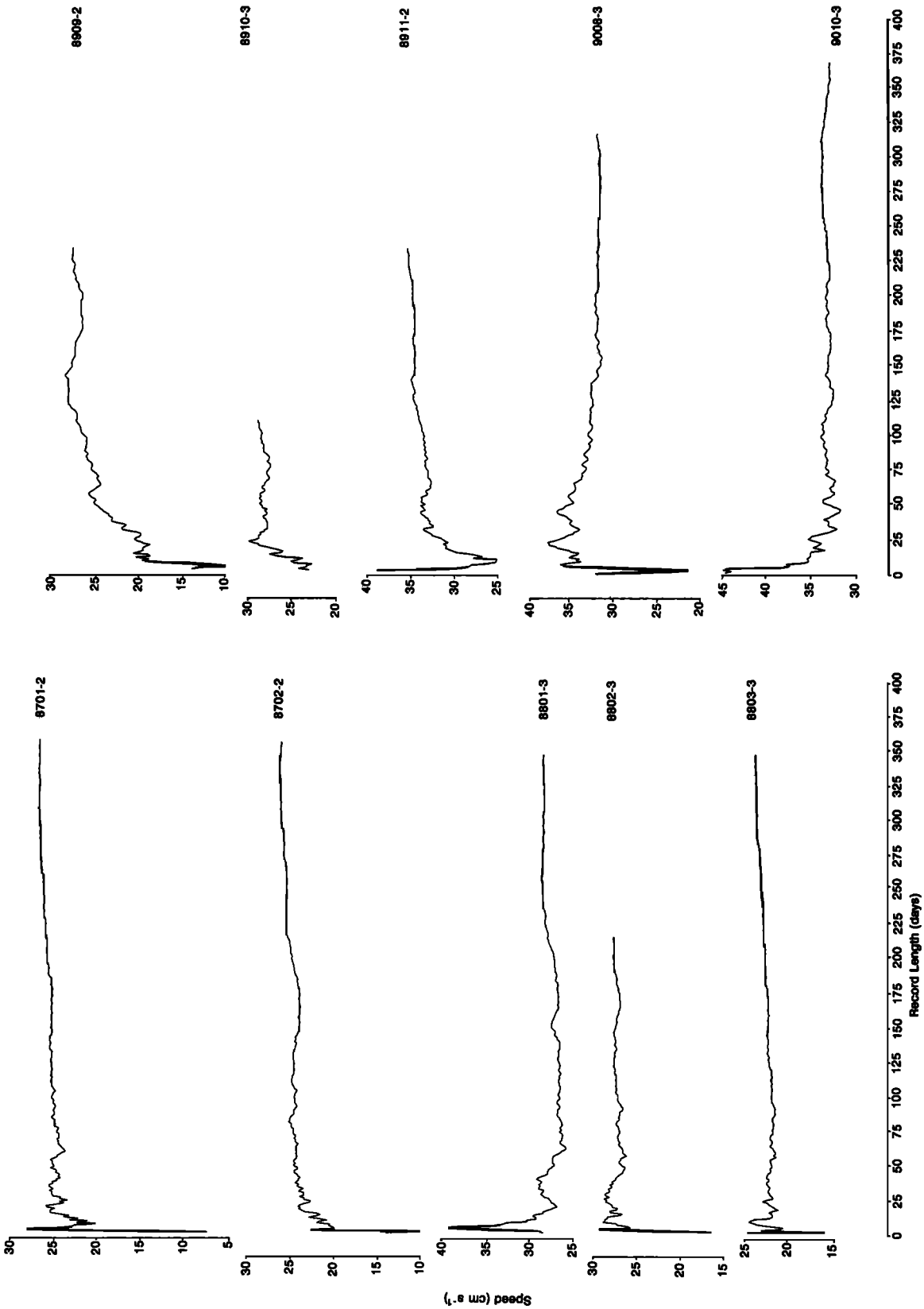

Figure 10. Mean near-bottom flow speeds for time intervals from 1 day to the full record length for 10 near-bottom records in the Denmark Strait Overflow. Instrument numbers are those listed in Table 2. For the instrument's relative location on the slope see Figure 11.

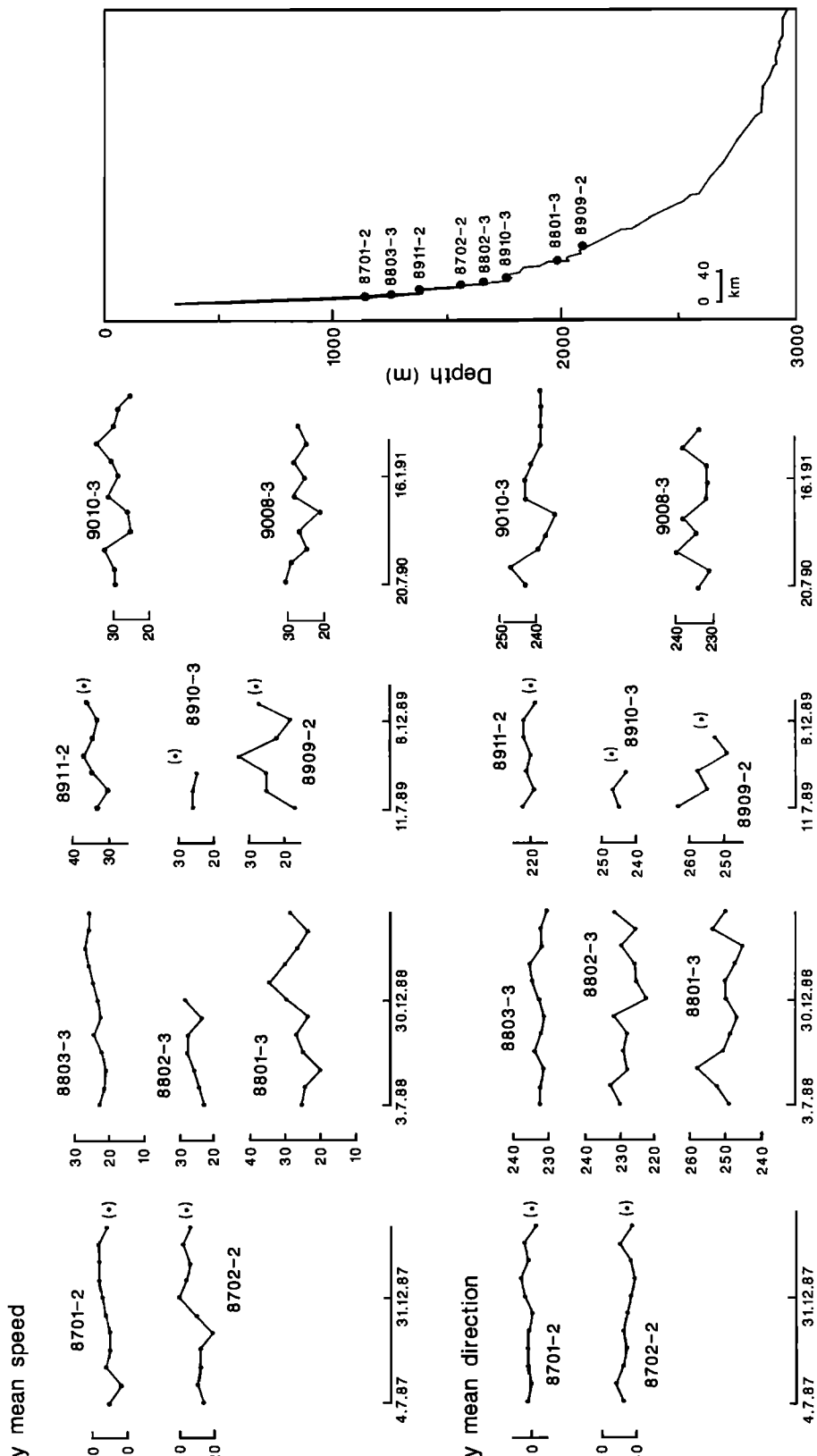

Figure 11. Thirty-day means of near-bottom current speed and direction in the Denmark Strait Overflow taken from successive deployments of instruments set at similar depths on the East Greenland Slope. The 87-, 88- and 89-series instruments are from the Angmagssalik array. The 90-series instruments are from equivalent depths on the TTO array.

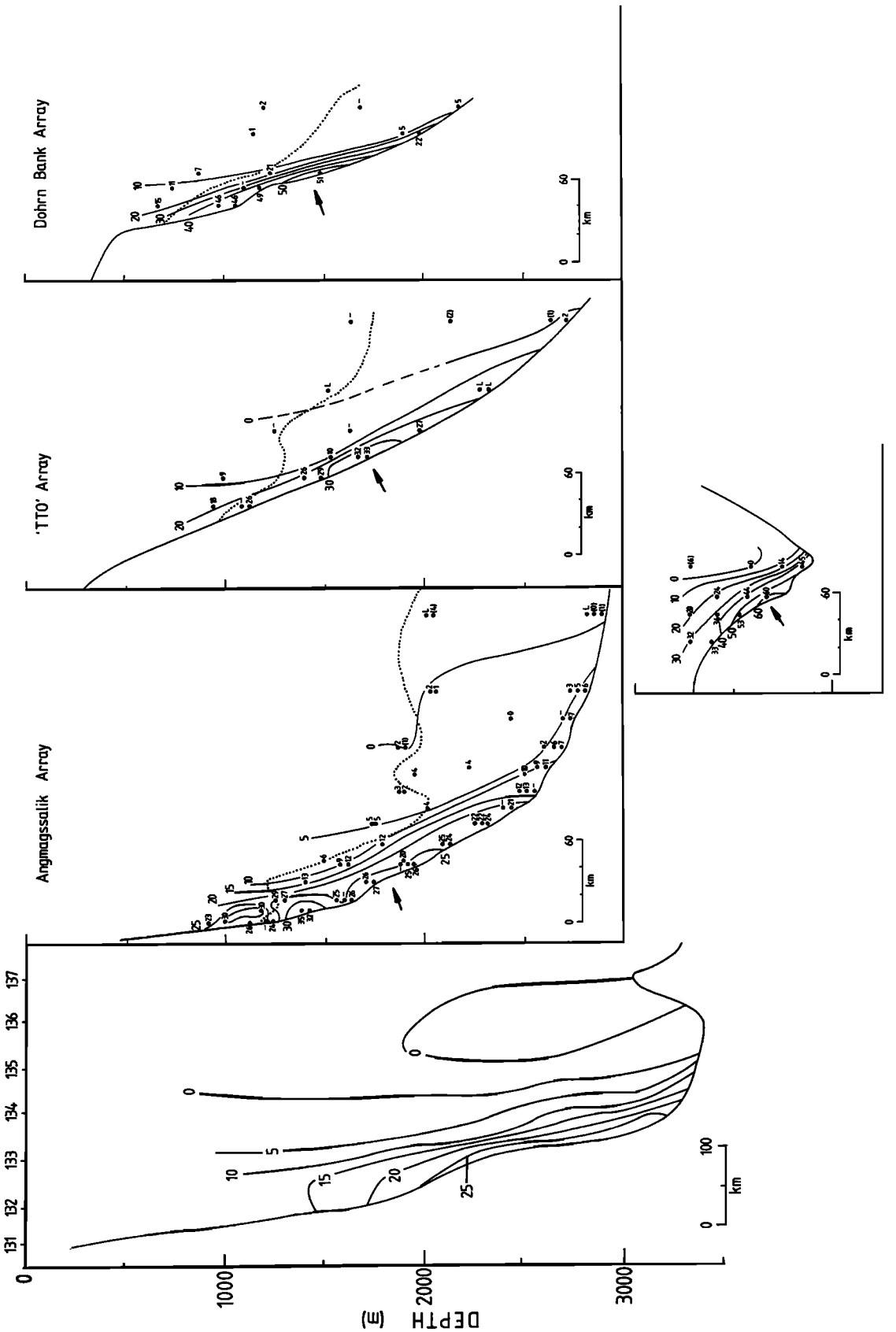

Figure 12. Distributions of mean current speeds (cm s^{-1}) on five arrays set normal to the Greenland Slope between a point 55 km south of the Denmark Strait sill [*Ross*, 1975] (inset) and Cape Farewell [*Clarke*, 1984]. Values in parentheses indicate flows to the north and east; all but the left-hand panel are to a common scale. Angmagssalik plot is a composite of data from all four deployments. Presumed core of the overflow current is indicated by arrows; dashed lines represent the approximate depth of the $\sigma\theta$ = 27.8 isopycnal on the three arrays, which lie at ~160-km intervals south of the sill. For locations, see Figure 4a.

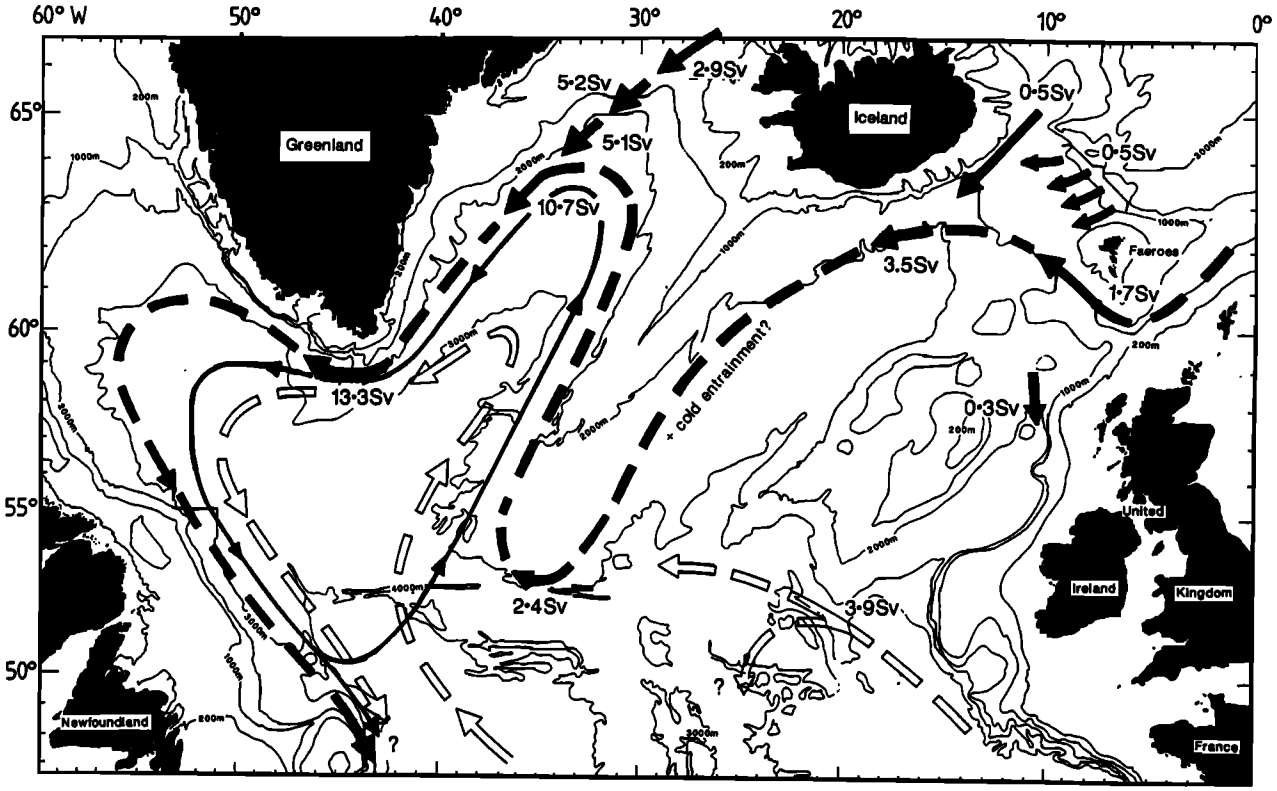

Figure 13. Proposed transport scheme for waters denser than $\sigma\theta = 27.80$ in the northern North Atlantic, based on all available measurements.

originated in the Denmark Strait. While it is certainly possible to find other estimates for the overflow transport at the Denmark Strait (as far back as *Worthington*'s [1969] estimate described earlier), the three estimates described above appear to be the most soundly based of their type; they are also independent and are in broad agreement. A representative figure of 2.9 Sv is therefore used to describe the Denmark Strait Outflow in Figure 13.

On the Dohrn Bank array and the TTO array, positioned at successive ~160-km intervals to the southwest of the sill (Figure 4), new transport estimates were derived by overlaying the isopycnal distribution obtained during deployment or recovery cruises onto the mean isotach distribution (Figure 12) and summing the transport for southwest going speeds of ≥ 0 and potential densities of ≥ 27.80. For the 109-day (nominal) Dohrn Bank array, the transport within these ranges amounted to 5.2 Sv, while the corresponding estimate for the 368-day TTO array was essentially identical at 5.1 Sv. The available evidence suggests, then, that much of the entrainment into the overflowing stream (in this case increasing its volume by a factor of 1.8) takes place close to the point of overflow, with a greatly reduced entrainment thereafter. These results appear to be in keeping with the output of the Baringer-Price descending plume model applied to this overflow (J. F. Price, personal communication, 1991; model described by *Baringer and Price* [1990]).

At a further ~160-km step to the southwest (Figure 4) the overflowing stream passes through the main Lowestoft array off Angmagssalik where a total of 60 current meters have been recovered over four deployments totalling almost 4 years. (A further two instruments were lost, and five of the instruments recovered provided no useful record; see Table 2.) In keeping with our earlier conclusions regarding the relative constancy of flow speeds over periods longer than a few tens of days, the mean speeds from all deployments of this array appear compatible and are plotted together in Figure 12. Only one set of data needed adjustment before plotting; the two moorings of the 1986 trial array were actually located 22 and 37 km, respectively, downstream from the eventual line of the Angmagssalik array. In projecting these values onto the plane of the main array, instrument depths were shallowed by 25 and 41 meters, respectively, to allow for the deepening of the overflow plume over the intervening distance. When the isotach distribution of Figure 12 is overlaid with the isopycnal distribution from the best (1988) conductivity temperature depth (CTD) coverage, the deep dense ($\sigma\theta \geq 27.80$) southwestward transport through the Angmagssalik array is estimated to be 10.7 Sv. (Regrettably, the initial recalculation for the full 60-instrument array, supplied to and reported by *McCartney* [1992, p. 286] was in error. The correct final transport estimate is 10.7 Sv as shown in his Figure 2 from *Dickson et al.* [1990].) Plainly then, a considerable accession to the dense along-slope transport has occurred at some point downstream from the TTO array (see Figure 13), and the scale of the increase (2.1 times) leaves no doubt that this change is real, not merely the result of differences in the date, duration, and instrumental density of our coverage. The possible sources of the increase will be discussed below.

Finally, along this inflow path, R. A. Clarke (personal

communication, 1991) has kindly recast his 1978 data set south of Cape Farewell in terms of the preferred density range of the present paper. For this site, ~740 km south of the Angmagssalik array, the deep dense transport at $\sigma\theta \geq 27.80$ is estimated to be 13.3 Sv (Figure 13).

The Northeastern Stream

In the northeast Atlantic the production of *Swift*'s [1984] Northeast Atlantic Deep Water (Figure 2) begins with flow through the Faroe Bank Channel. We have several estimates of the cold outflow there that are individually poorly based but that are in reasonably close agreement. *Crease* [1965] calculated the through flow of Norwegian Sea Deep Water to be 1.8 Sv, based on a combination of direct float measurements at 760 m depth and hydrography. Both *Saetre* [1967] and, later, *Borenäs and Lundberg* [1988] used short-term fixed point current measurements (Aanderaa and Pisa, respectively) and hydrography to derive identical estimates of 1.5 Sv for the cold water flux (<3°C); the latter authors note that this value conforms with the expectations of simple hydraulic theory for controlled flow through a constriction with parabolic topography.

Saunders [1990] then contributed the first long direct current measurements to the calculation. Combining a 4 1/2-month and a 12-month record from the cold outflow with estimates of its cross-sectional area based on three short-term CTD/acoustic Doppler current profiler sections, Saunders calculates the flux of cold water <3°C to be 1.9 ± 0.4 Sv, with a further minor overspill of ~0.3 Sv escaping south to the Rockall Trough via a notch in the Wyville-Thompson Ridge, in conformity with an earlier estimate by *Ellett and Edwards* [1978]. (3°C corresponds to a density of $\sigma\theta = 27.9$. However, recalculating the cold water flux for densities ≥27.8 leads to only a marginal increase of ~0.1 Sv; P. M. Saunders (personal communication, 1993.)

In the presence of an energetic high-frequency variability these estimates are to all intents and purposes identical and they are given a representative mean value of 1.7 Sv in the dense-water transport scheme shown in Figure 13.

For the area immediately to the west, *Meincke* [1983] has provided our only estimate of the dense water which overspills the Greenland-Scotland Ridge through deep notches in the ridge crest between Iceland and Faroe. From an analysis of water mass distributions plus some local current measurements, Meincke estimates the total cold overspill at 1 Sv, with 0.5 Sv using the main cross-ridge channel immediately east of Iceland and the remainder trickling through four lesser notches further east (data transferred without alteration to Figure 13).

We can anticipate that the Iceland-Scotland overflows might be augmented from two main sources as they pass through the south Icelandic Basin en route to the Charlie-Gibbs Fracture Zone:

First, such vigorous overflows as *Borenas and Lundberg* [1988] and *Saunders* [1990] describe for the Faroe Bank Channel, with short-term measurements of flow exceeding 100 cm s^{-1}, some evidence of billow turbulence, and turbulent diffusivities ranging upward to 150 cm^2 s^{-1}, must involve a considerable warm entrainment of local water. Such entrainment seems evident in the early observations of *Steele et al.* [1962] and *Worthington and Volkmann* [1965] that these overflows had swollen to an estimated 5 Sv where they pass south of Iceland; however, the very recent recovery of a 7-mooring 1-year array by P. M. Saunders (unpublished data, 1993) from the same location has provided us with a longer term and therefore more reliable estimate of 3.5 Sv for transport at $\sigma\theta \geq 27.8$ south of Iceland. (We are indebted to P. M. Saunders for permission to include this unpublished estimate in Figure 13).

The second potential contributor to NADW production in the eastern basin has its origins in the high-silicate, low-oxygen, low-salinity Antarctic Bottom Water (AABW) derivative which *McCartney* [1992] describes passing into the Eastern Basin through the Vema Fracture Zone at 11°N. Of the 4–5 Sv of AABW which spreads northward across the equator, about half (2.1–2.5 Sv) diverts east through the Vema Fracture Zone and spreads north, initially against the western and later against the eastern margin of the Eastern Basin [*McCartney et al.*, 1991; *Saunders*, 1987] warming as it spreads. Around 1.9 Sv of this warmer LDW derivative is estimated by *McCartney* [1992] to pass north through 36°N. As it continues north, this LDW component of southerly origin augments the deep recirculating cyclonic gyre of the West European Basin with the result that a total flow of 3.9 Sv at $\sigma\theta \geq 27.8$ is estimated by *McCartney* [1992] to turn westward through 20°W at the head of the basin. As *McCartney* [1992, p. 376] points out "this combines with the eastern overflows [i.e., 2.7 Sv as in Figure 13] to give an estimated 6.6 Sv to flow west through the CGFZ, exclusive of any warm water entrainment downstream of the overflow measurements or LSW entrainment across the 27.8 isopycnal."

Although the dramatic increase (2.1 times) in the dense water flux between our TTO and Angmagssalik arrays plainly demands some new source of this magnitude, and although a deep flow adequate to meet that demand is evidently delivered through the Eastern Basin towards the CGFZ, nothing like that amount is observed to pass through. The sixteen 400-day current meter records recovered by *Saunders* [this issue] from an 8-mooring north-south array across the snout of the Reykjanes Ridge and CGFZ, slightly west of the sill, were well placed to monitor the saline core in the range 34.94–34.975, which marks the overflow water in this region and which corresponds approximately to our chosen density interval of $\sigma\theta \geq 27.8$ (or $\sigma_2 = 36.925$ [*Saunders*, this issue]). For water of these characteristics, Saunders reports an unsteady through flow (in marked contrast to the overflows at source) and a lack of a seasonal signal (following *Harvey* [1980]), but a record mean flux of only 2.4 ± 0.5 Sv, much less than all previous estimates based on hydrography alone.

Though no coverage in such complex topography can be regarded as complete, *Saunders* [this issue] points out that changing the method of defining the overflow leads to only minor differences in the transport, so that it is difficult to see how improved coverage could significantly alter the transport estimate. The fate of the "excess" Eastern Basin deep-water production reported by *McCartney* [1992] is not known; if real, it is presumably either mixed out or recirculated within the Eastern Basin.

The Balance

Though the sparsity of direct measurements means that present transport schemes must remain tentative, they are gradually improving beyond speculation, anchored at certain key locations by direct flow measurements of some ade-

quacy. As *Saunders* (this volume) points out, such long-term arrays are necessary to distinguish the long-term mean transport from its short-term fluctuations. To this role in controlling estimates based on short-term hydrography we would add a further role in validating the estimates from shorter-term current meter arrays.

As a present-day interpretation of how the deep-transport scheme might be, Figure 13 is at least controlled by most of the available direct measurements and covers a consistent density interval ($\sigma\theta \geq 27.8$), but large uncontrolled or unquantifiable areas remain, and for these our intention has been to balance the budget in the simplest way compatible with hydrography. Fortunately, *McCartney*'s [1992] exhaustive and considered review of the modern hydrographic record provides a clear indication as to where any imbalances might be met. He points to three main sources. The first and shallowest is a recirculating loop of Labrador Sea Water (LSW) whose lower layers are of a sufficient density to contribute to the transport passing our arrays but which, as a true recirculation, will not contribute to the net southward flux of the Deep Western Boundary Current (DWBC). The second is a cold entrainment bleeding from this LSW layer into the dense overflows below, and which would therefore be lost southward in the DWBC. As *McCartney* [1992, p. 286] points out, such a cold entrainment is necessary to maintain the overflows at their observed temperature.

These two LSW components are represented by a continuous bold line in Figure 13, with the arrow at its southern bound representing the net loss southward. (A similar recirculation and cold entrainment are also indicated for the Eastern Basin in *McCartney*'s [1992, Figure 8], scheme but the measured interbasin exchange appears so weak (see above) that they are omitted from Figure 13.)

The third source underscored by McCartney is a recirculating component of Lower Deep Water derived from the northward spread of AABW through the Western Basin. From its obvious high-silicate, low-salinity, low-oxygen characteristics, McCartney shows this component to participate in a cyclonic loop at the head of the Western Basin, spreading north in contact with the bottom along the western flanks of the Mid-Atlantic Ridge and returning south as an off-bottom layer undercut by and exchanging with the low-silicate, high-oxygen product of the northern overflows where they follow a parallel course east of Newfoundland. The path of this LDW loop is indicated by open arrows in Figure 13. Unfortunately, while its course is known, its net transport is not since it is masked by a probable cyclonic recirculation of much greater magnitude [*McCartney*, 1992].

The imbalances that these three components are required to meet are clear from Figure 13. Off east Greenland, the fully developed Denmark Strait overflow and CGFZ throughflow contribute 7.5 Sv to an observed transport of 10.7 Sv off Angmagssalik, leaving a shortfall of some 3.2 Sv. All of this is assumed to be of LSW origin for a number of reasons: (1) If present at these latitudes, any LDW component could only occur at the deepest part of the slope, but in these depths off Angmagssalik, A. Watson et al. (unpublished manuscript, 1994) show almost pure Denmark-Strait-origin water. (2) The full measured contribution of the CGFZ throughflow, including its Iceland-Scotland overflow component, has already been accounted for. (3) The expansion of the high-speed core of the current between the TTO and Angmagssalik arrays is toward the upper part of the slope, not the lower. (Compare the relevant isotach distributions in Figure 12.) In the upper part of that high-speed along-slope flow but below the point at which the $\sigma\theta = 27.80$ isopycnal intersected the slope in July 1988 and 1989 (i.e., 1300–1600 m), the tracer properties show only a slight admixture of water from the Denmark Strait. (4) *McCartney* [1992, p. 298] quotes a personal communication from R. A. Clarke in which he estimates that a similar quantity (4.3 Sv) of the 13.3 Sv transport rounding Cape Farewell consists of water with Labrador Sea Water characteristics. (*Clarke* [1984] had earlier estimated the strength of the LSW recirculation loop at ~4 Sv.) An LSW origin for the transport imbalance off Angmagssalik therefore appears most likely, though we are unable to partition this LSW contribution into its recirculating and entraining components.

Between the Angmagssalik array and Cape Farewell the estimated transport at $\sigma\theta \geq 27.8$ increases by an additional 2.6 Sv. The transport scheme of Figure 13 suggests that this relatively small residual imbalance is due to a growing contribution from the deep LDW loop south of Greenland, perhaps with some further contributions from any LSW short circuit not picked up by our Angmagssalik array.

Thus it seems probable that the imbalances between our points of direct measurement are of an order which can easily be met by the deep recirculating flows of the Western Basin, though refining their net contribution to the transport of the DWBC will require the partitioning of each flow into its net southgoing and recirculating components, and these are not known at the present time.

Such considerations should not be allowed to obscure the fact, however, that after a considerable observational and analytical effort, the recent scientific literature is converging on a consistent zero-order description for NADW production and pathways. For what might be termed its early developmental stages in the northern North Atlantic, we believe that the estimates provided here, building from a total of 5.6 Sv at the points of overflow to around 13.3 Sv at Cape Farewell, are both self-consistent and adequately controlled by direct current measurement.

From Cape Farewell southward, the consistency is maintained. In their wide-ranging review, *Schmitz and McCartney* [1993] point out that although the southgoing transport of NADW may swell to 2–3 times its "new" production (i.e., 35–40 Sv) where it merges temporarily with the great recirculations south of the Gulf Stream and along the coast of northeast Brazil, they nevertheless find an astonishing consistency in the following key determinations: that *Roemmich* [1980] found 14 Sv to be the net abyssal transport south through 24°N; that in the South Atlantic, *Rintoul* [1991] found a net abyssal transport of 13 Sv passing south through 32°S (17 Sv of NADW flowing south, less 4 Sv of AABW flowing north); that Rintoul's scheme compensates for all of this southward abyssal outflow with a 13 Sv inflow from the Drake Passage at thermocline and intermediate depths; and that at equivalent thermocline depths (warmer than 7°C) *Schmitz and Richardson* [1991] found a total of 13 Sv of South Atlantic origin passing north through the Florida Straits.

Though differences remain (e.g., in the size of the CGFZ throughflow and hence in the wider significance of deep water production in the Eastern Basin), we would concur with *Schmitz and McCartney*'s [1993] judgement that a

consistent pattern of NADW circulation is emerging. We would also agree that this consistency does not imply a diminishing role for direct observations.

4. Conclusions

The production of NADW is one of the key variables which determine the Earth's response to climate change, acting to moderate the global redistribution of heat and salt. NADW production is itself most vulnerable to change in the northern North Atlantic where the processes controlling deep water mass conversion are at their most direct. Within the density range considered here ($\sigma\theta \geq 27.80$) NADW has four main sources: the dense overflows from intermediate depths in the Nordic Seas (*Swift*'s [1984] NEADW and NWABW); the lower part of the LSW layer including both a recirculating and an entraining component, and a recirculating AABW derivative (*McCartney*'s [1992] LDW) of southerly origins in the deepest layers of either basin. From recent observations by ourselves and others we draw the following conclusions relevant to the production and circulation of NADW:

1. Direct current measurements, mainly from the Denmark Strait Overflow, suggest the following characteristics for the overflow streams in their present-day state. Fast (up to 60 cm s^{-1} in the long-term mean), thin (100–150 m) flows following topography with intense near-bottom shear (K_M increasing by over 4 orders of magnitude over a few hundred meters depth just south of Denmark Strait), an energetic dominant variability timescale of a few (normally 1–12) days with amplitude similar to that of the mean but relatively invariant at longer timescales (no seasonal signal), with a maximum entrainment close to source and a nonlinear deceleration and deepening downstream (known for the Denmark Strait overflow only) as a result of frictional effects.

2. The total direct transport of these overflows from intermediate depths amounts to ~5.6 Sv, equally divided east and west of Iceland. In the case of the Denmark Strait Overflow its 2.9 Sv increases rapidly by entrainment to 5.2 Sv where it passes Dohrn Bank 160 km downstream from the sill but thereafter with reduced entrainment and constant transport to our TTO array (5.1 Sv) a further 160 km downstream. At some point between the TTO and Angmagssalik arrays the deep transport at $\sigma\theta \geq 27.8$ once again shows a rapid increase, doubling to 10.7 Sv as other NADW components merge with the overflow. While the production of deep water in the Eastern Basin (dense overflows plus warm entrainment plus cold LSW entrainment plus LDW) seems more than adequate to contribute the difference, in fact the CGFZ throughflow appears to restrict this contribution to ~2.4 Sv. The balance of 3.2 Sv and the further slight increase observed between Angmagssalik and Cape Farewell are attributed to the three deep Western Basin sources identified by *McCartney* [1992]: LSW recirculation, cold entrainment from the LSW layer, and the LDW loop of southern origins.

3. Though we cannot yet partition these last three contributions into their recirculating and net southgoing components, the figure of approximately 13 Sv for the almost-developed NADW transport as it rounds Cape Farewell looks to be a sensible one. The recent review by *Schmitz and McCartney* [1993] highlights the fact that a net abyssal flow of about this order (17 Sv NADW minus 4 Sv AABW [*Rintoul*, 1991]) passes south through the South Atlantic, while a net flow of 13 Sv from the South Atlantic passes north through the Florida Straits at thermocline depths, apparently in compensation.

Acknowledgments. The primary stimulus for this work was a review by Peter Saunders of IOS Deacon Laboratory in the spring of 1986 which made a compelling case for direct measurements of the principal overflows. It is also a pleasure to acknowledge the contribution of the scientists and crews of R/V *Cirolana*, *Bjarni Saemundsson*, *Anton Dohrn*, and *Aranda* in sustaining such an extended mooring program in difficult conditions off Greenland. We thank Svend-Aage Malmberg, Jens Meincke, and Pentti Malkki for their help in making it happen. This paper is a contribution of the UK WOCE program.

References

Aagaard, K., and E. C. Carmack, The role of sea ice and other fresh water in the Arctic circulation, *J. Geophys. Res.*, *94*, 14,485–14,498, 1989.

Aagaard, K., and S.-A. Malmberg, Low frequency characteristics of the Denmark Strait overflow, *ICES CM 1978/C:47*, Int. Counc. for the Explor. of the Sea, Copenhagen, 1978.

Baringer, M. O., and J. F. Price, A simple model of the descending Mediterranean outflow plume, *The Physical Oceanography of Sea Straits*, edited by L. J. Pratt, pp. 537–544, *NATO ASI Ser., C, 318*, 1990.

Borenäs, K. M., and P. A. Lundberg, On the deep water flow through the Faroe Bank Channel, *J. Geophys. Res.*, *93*, 1281–1292, 1988.

Bowden, K. F., The dynamics of flow on a submarine ridge, *Tellus*, *12*(4), 418–426, 1960.

Broecker, W. S., and G. H. Denton, The role of ocean-atmosphere reorganisations in glacial cycles, *Geochim. Cosmochim. Acta*, *53*, 2465–2501, 1989.

Broecker, W. S., and T.-H. Peng, *Tracers in the Sea*, 690 pp., Lamont-Doherty Earth Observatory, New York, 1982.

Cartwright, D. E., On the smoothing of climatological time-series with application to sea-level at Newlyn, *Geophys. J. R. Astron. Soc.*, *75*, 639–658, 1983.

Charles, C. D., and R. G. Fairbanks, Evidence from Southern Ocean sediments for the effect of North Atlantic deep water flux on climate, *Nature*, *355*, 416–419, 1992.

Clarke, R. A., Transport through the Cape Farewell-Flemish Cap section, *Rapp. P. V. Réun. Cons. Int. Explor. Mer*, *185*, 120–130, 1984.

Crease, J., The flow of Norwegian Sea water through the Faroe Bank Channel, *Deep Sea Res.*, *12*, 143–150, 1965.

Dickson, R. R., Flow statistics from long-term current meter moorings: The global data-set in January 1989, *WMO/TD-337*, World Meteorol. Org., Geneva, 1990.

Dickson, R. R., E. M. Gmitrowicz, and A. J. Watson, Deep water renewal in the northern North Atlantic, *Nature*, *344*, 848–850, 1990.

Ellett, D. J., and A. Edwards, A volume transport estimate for Norwegian Sea overflow across the Wyville-Thomson Ridge, *ICES CM 1978/C:19*, Int. Counc. for the Explor. of the Sea, Copenhagen, 1978.

Foldvik, A., and T. Gammelsrod, Notes on Southern Ocean hydrography, sea-ice and bottom water formation. *Palaeogeogr. Palaeoclimatol. Palaeoecol.*, *67*, 3–17, 1988.

Gould, W. J., J. Loynes, and J. Backhaus, Seasonality in slope current transports NW of Shetland, *ICES CM 1985/C:7*, Int. Counc. for the Explor. of the Sea, Copenhagen, 1985.

Harvey, J. G., Deep and bottom water in the Charlie-Gibbs Fracture Zone, *J. Mar. Res.*, *38*, 173–182, 1980.

Jones, S. R., and J. W. Read, MAFF current meter system and data inventory, 1987–89, *Fisheries Res. Tech. Rep. 94*, 28 pp., Minist. of Agric. Fish. and Food, Direct. Fish. Res., Lowestoft, England, 1993.

Livingston, H. D., J. H. Swift, and H. G. Ostlund, Artificial

radionuclide tracer supply to the Denmark Strait Overflow between 1972 and 1981, *J. Geophys. Res.*, *90*, 6971–6982, 1985.
McCartney, M. S., Recirculating components to the deep boundary current of the northern North Atlantic, *Prog. Oceanogr.*, *29*, 283–383, 1992.
McCartney, M. S., and L. D. Talley, Warm-to-cold water conversion in the northern North Atlantic Ocean, *J. Phys. Oceanogr.*, *14*, 922–935, 1984.
McCartney, M. S., S. L. Bennett, and M. E. Woodgate-Jones, Eastward flow through the Mid-Atlantic Ridge at 11°N and its influence on the abyss of the eastern basin, *J. Phys. Oceanogr.*, *21*, 1089–1121, 1991.
Meincke, J., The modern current regime across the Greenland-Scotland ridge, in *Structure and Development of the Greenland-Scotland Ridge*, edited by A. Bott et al., pp. 637–650, Plenum, New York, 1983.
Pillsbury, R. D., D. Barstow, J. S. Bottero, C. Milleiro, B. Moore, G. Pittock, D. C. Root, J. Simpkins, III, R. E. Still, and H. L. Bryden, Gibraltar experiment: Current measurements in the Strait of Gibraltar, October 1985–October 1986, *rep. 87-29*, 284 pp., College of Oceanography, Oregon State Univ., Corvallis, Oregon, 1987.
Price, J. F., M. T. O'Neil-Baringer, R. G. Lueck, G. C. Johnson, I. Ambar, G. Parilla, A. Cantos, M. A. Kennelly, and T. B. Sanford, Mediterranean outflow mixing and dynamics, *Science*, *259*(5099), 1277–1282, 1993.
Rintoul, S. R., South Atlantic interbasin exchange, *J. Geophys. Res.*, *96*, 2675–2692, 1991.
Roemmich, D., Estimation of meridional heat flux in the North Atlantic by inverse methods, *J. Phys. Oceanogr.*, *10*, 1972–1983, 1980.
Ross, C. K., Overflow 73, current measurements in Denmark Strait, *ICES CM 1976/C:6*, Int. Counc. for the Explor. of the Sea, Copenhagen, 1975.
Ross, C. K., Overflow 73: Transport of overflow water through Denmark Strait, *ICES CM 1976/C:16*, Int. Counc. for the Explor. of the Sea, Copenhagen, 1976.
Ross, C. K., Overflow 73, Moored instrument time series, vol. 2, BIO Data Ser. *BI-D-77-5*, 187 pp., Bedford Inst. of Oceanogr., Dartmouth, Nova Scotia, Canada, 1977.
Ross, C. K., Overflow variability in Denmark Strait, *ICES CM 1978/C:21*, Int. Counc. for the Explor. of the Sea, Copenhagen, 1978.
Ross, C. K., Characteristics of overflow water in Denmark Strait, *ICES CM 1983/C:7*, Int. Counc. for the Explor. of the Sea, Copenhagen, 1983.
Ross, C. K., Temperature-salinity characteristics of the 'overflow' water in Denmark Strait during 'OVERFLOW '73', *Rapp. P. V. Reun. Cons. Int. Explor. Mer*, *185*, 111–119, 1984.
Saetre, R., Report on the Norwegian investigations in the Faroe Channel, 1964–65, *38*, NATO Subcom. on Oceanogr. Res., Brussels, 1967.
Saunders, P. M., Flow through Discovery Gap, *J. Phys. Oceanogr.*, *17*, 631–643, 1987.
Saunders, P. M., Cold outflow from the Faroe Bank Channel, *J. Phys. Oceanogr.*, *20*, 29–43, 1990.
Saunders, P. M., The flux of overflow water through the Charlie-Gibbs Fracture Zone, this issue.
Schmitz, W. J., Jr., and M. S. McCartney, On the North Atlantic Circulation, *Rev. Geophys.*, *31*, 29–49, 1993.
Schmitz, W. J., Jr., and P. L. Richardson, On the sources of the Florida Current, *Deep Sea Res.*, *38*, suppl. 1, S389–S409, 1991.
Smith, P. C., A streamtube model for bottom boundary currents in the ocean, *Deep Sea Res.*, *22*, 853–873, 1975.
Smith, P. C., Baroclinic instability in the Denmark Strait overflow, *J. Phys. Oceanogr.*, *6*, 355–371, 1976.
Steele, J. H., J. R. Barrett, and L. V. Worthington, Deep currents south of Iceland, *Deep Sea Res.*, *9*, 465–474, 1962.
Swift, J. H., The circulation of the Denmark Strait and Iceland-Scotland overflow waters in the North Atlantic, *Deep Sea Res.*, *31*, 1339–1355, 1984.
Swift, J. H., K. Aagaard, and S.-A. Malmberg, The contribution of the Denmark Strait overflow to the deep North Atlantic, *Deep Sea Res.*, *27*, 29–42, 1980.
Talley, L. D., and M. S. McCartney, Distribution and circulation of Labrador Sea Water, *J. Phys. Oceanogr.*, *12*, 1189–1205, 1982.
Warren, B. A., Deep circulation of the world ocean, in *Evolution of Physical Oceanography*, edited by B. A. Warren and C. Wunsch, pp. 6–41, MIT Press, Cambridge, Mass., 1981.
Whitehead, J. A., M. E. Stern, G. R. Flierl, and B. A. Klinger, Experimental observations of baroclinic eddies on a sloping bottom, *J. Geophys. Res.*, *95*, 9585–9610, 1990.
Worthington, L. V., An attempt to measure the volume transport of Norwegian Sea overflow water through the Denmark Strait, *Deep Sea Res.*, *16*(suppl.), 421–432, 1969.
Worthington, L. V., The Norwegian Sea as a Mediterranean basin, *Deep Sea Res.*, *17*, 77–84, 1970.
Worthington, L. V., On the North Atlantic circulation, *Johns Hopkins Oceanogr. Stud.*, *6*, 110 pp., 1976.
Worthington, L. V., and G. H. Volkmann, The volume transport of the Norwegian Sea overflow water in the North Atlantic, *Deep Sea Res.*, *12*, 667–676, 1965.
Worthington, L. V., and W. R. Wright, North Atlantic Ocean atlas of potential temperature and salinity in the deep water including temperature, salinity and oxygen profiles from the ERIKA DAN cruise of 1962, *Woods Hole Oceanogr. Inst. Atlas Ser.*, vol. 2, Woods Hole, Mass., 1970.
Wunsch, C., Decade-to-century changes in the ocean circulation, *Oceanography*, *5*(2), 99–106, 1992.

J. Brown and R. R. Dickson, Fisheries Laboratory, Directorate of Fisheries Research, Ministry of Agriculture, Fisheries, and Food, Lowestoft NR33 0HT, Suffolk, England.

(Received December 2, 1992; revised June 21, 1993; accepted July 19, 1993.)